CCFE
CULHAM CENTRE FOR FUSION ENERGY

UK Atomic Energy Authority

UKAEA-CCFE-PR(25)405

H. G. Dudding, F. J. Casson, D. Dickinson, C. M. Roach, B. S. Patel, E. Delabie, C. F. Maggi, P. Rodriguez-Fernandez, M. F. F. Nave, JET contributors

# Integrated modelling simulations of Ohmic and L-mode JET discharges in H, D and T using JETTO-TGLF

# Integrated modelling simulations of Ohmic and L-mode JET discharges in H, D and T using JETTO-TGLF

H. G. Dudding, F. J. Casson, D. Dickinson, C. M. Roach, B. S. Patel,
E. Delabie, C. F. Maggi, P. Rodriguez-Fernandez, M. F. F. Nave,
JET contributors

This is a preprint of a paper submitted for publication in
Plasma Physics and Controlled Fusion

# Integrated modelling simulations of Ohmic and L-mode JET discharges in H, D and T using JETTO-TGLF

**H.G. Dudding[1,*], F.J. Casson[1], D. Dickinson[2], C.M. Roach[1], B.S. Patel[1], T.W. Bache[1], E. Delabie[3], C.F. Maggi[1], P. Rodriguez-Fernandez[4], M.F.F. Nave[5], JET Contributors[†] and the EUROfusion Tokamak Exploitation Team[$]**

[1]UKAEA, Culham Campus, Abingdon, Oxfordshire, OX14 3DB, UK
[2]York Plasma Institute, University of York, Heslington, York, YO10 5DD, UK
[3]Oak Ridge National Laboratory, Oak Ridge, TN 37831, United States of America
[4]MIT Plasma Science and Fusion Center, Cambridge, MA 02139, United States of America
[5]Instituto de Plasmas e Fusão Nuclear, Instituto Superior Técnico, Universidade de Lisboa, Lisboa, P1049-001, Portugal
[†]See the author list of C.F. Maggi *et al* 2024 *Nucl. Fusion* **64** 112012
[$]See the author list of E. Joffrin *et al* 2024 *Nucl. Fusion* **64** 112019
[*]Email: harry.dudding@ukaea.uk

**Abstract**

The ability to capture the isotope mass scaling of core confinement seen in experiment is validated with JETTO-TGLF for low power JET-ILW discharges across H, D and T. The cases analysed include Ohmic discharges spanning the linear and saturated Ohmic confinement regimes as well as a trio of L-modes. The TGLF saturation rules SAT1-SAT3 are seen to predict a similar isotope scaling across both the ITG- and TEM-dominated discharges simulated, despite for the latter case the inclusion of the TEM branch of SAT3. The models demonstrate good agreement with experiment for the scaling between D and T plasmas, however a discrepancy is observed for H in the ITG-dominated discharges of higher density, as well as a systematic overprediction of the confinement time on the order of 20% in most cases. A retuned version of the SAT3 model, which was fit to better recreate fluxes close to the transport threshold, is seen to improve the magnitude of confinement predictions across all shots owing to an increased transport stiffness. This retuning was not seen to influence the confinement isotope scaling however, and possible transport mechanisms responsible for the continued discrepancy of higher density Ohmic and L-mode discharges in H are discussed.

## 1 Introduction

In the pursuit of making global confinement predictions of tokamak plasmas one typically requires the use of integrated modelling codes, such as JETTO [1] and ASTRA [2]. These comprise a suite of models each simulating a different aspect of the tokamak, which interact self-consistently to describe the evolution of the plasma profiles on confinement timescales [3]. A key ingredient to these frameworks is the reduced turbulence model, due to turbulence typically forming the dominant transport mechanism in a tokamak plasma. 'Reduced' here is in reference to its relative simplicity in comparison to the higher fidelity paradigm of nonlinear gyrokinetics [4, 5], the use of which as a transport model is generally infeasible due to its computational expense[1]. The aim of reduced models is to approximate the level of turbulent transport expected from nonlinear gyrokinetic simulations for a given plasma state however using a fraction of the computational cost. Reduced models can range from the comparatively simple, such as Bohm-gyroBohm diffusion [8], to more complex quasilinear codes like QuaLiKiz [9, 10] and TGLF [11–13]. This latter class of model calculates turbulent fluxes via the combination of a linear solver and a saturation rule [14], which is a semi-empirical function with grounding in theory that takes information from the linear physics and uses it to describe the nonlinearly-saturated turbulent fluctuation spectra. This approach allows for an agreeable trade-off between accuracy and computational cost, with current research into machine learning surrogates for quasilinear models aiming to bring this cost down even further [15–17].

During the course of developing a saturation rule, such as the mixing length rule used in QuaLiKiz [18] and the paradigm of zonal mixing employed by TGLF's SAT1-SAT3 [19–21], one typically generates a selection of free parameters that are tuned to a database of nonlinear gyrokinetic simulations. This aspect of quasilinear models leaves them susceptible to a common problem of proxy models: their regimes of validity can be restricted

[1]We note that integrated modelling simulations using nonlinear gyrokinetics as a transport solver are being performed [6, 7], however are not yet routine.

to the parameter space on which they have been developed. Due to their imperfect recreation of nonlinear simulation data and the vast dimensionality of the local gyrokinetic input space, quasilinear saturation models can be regarded as being in a cycle of development. Namely, suppose that a discrepancy is found between the predictions of integrated modelling and experiment. Stand-alone comparisons can then be made between nonlinear gyrokinetic simulations and our reduced turbulence models to identify the origin of the discrepancy, allowing improvements to the reduced models to be developed. These improvements can then be verified and validated in integrated modelling simulations, until a further discrepancy is found, at which point the cycle repeats. By continuing this process, one aims to generate models with strong applicability in wider and wider ranges of parameter space. As an example, a focus historically has been on the development of models applicable to large aspect ratio tokamaks covering turbulence regimes dominated by electrostatic transport, typically with a lack of emphasis on shaping parameters. Such conditions are not expected in a spherical tokamak [22, 23] such as STEP [24], and so a saturation rule was recently developed to address the calculation of transport in regimes of strongly shaped, electromagnetic turbulence [25].

Another example of this process was the development of TGLF-SAT3 [21], which was motivated by observations that the scaling of confinement time $\tau_{\mathrm{E}}$ with isotope mass $A$ in experiment differed from that predicted using simple theory arguments. Said arguments put forward that local turbulent heat transport $Q$ follows gyroBohm scaling, such that $Q \propto \sqrt{A}$. This suggests that the confinement time would decrease with increasing isotope mass, however the opposite $\tau_{\mathrm{E}} \propto A^p$, $p > 0$ is often seen experimentally [26–30]. While transport in local nonlinear gyrokinetic simulations can regularly be seen to follow gyroBohm-like scaling in regimes of ITG turbulence [31–33], the so-called anti-gyroBohm scaling $Q \propto A^\alpha$, $\alpha < 0$, can be found in other regimes, such as turbulence dominated by TEM [34]. A comparison of contemporary quasilinear models with nonlinear gyrokinetic simulations in this regime [21] found a gyroBohm-like scaling for them all, indicating that the physics of TEM saturation was not being captured in the reduced models. SAT3 was therefore developed to include this anti-gyroBohm scaling effect, using a model for disparate saturation levels depending on whether the dominant mode was ITG or TEM. The saturation model quantities were related to the linear physics using a paradigm similar to zonal mixing, which forms the basis of previous TGLF saturation rules, thus representing an incremental step in the development cycle. Presented as a model for ion-scale turbulence in [21], the unification with the electron-scale physics of SAT2 is discussed in [35]. TGLF-SAT3 has since been used in several integrated modelling studies [36–38], and is seen to perform well in comparison to higher fidelity models and other saturation rules.

In this work a validation effort of SAT1-SAT3 is presented, comparing their abilities to recreate the isotope scaling of confinement seen in experiment through integrated modelling simulations. To this end, a selection of JET-ILW Ohmic and L-mode discharges in H, D and T have been chosen to compare with predictive simulations using JETTO-TGLF. The focus on low-power pulses was chosen for this work in part due to the inclusion of SAT3, owing to the greater influence of TEM in low-density Ohmic discharges [39, 40][2]. The rest of this paper is organised as follows: Section 2 describes the experimental discharges chosen for this work, as well as the setup for the integrated modelling simulations. The results of the predictive simulations obtained with the different TGLF saturation rules are presented in Section 3. In Section 4 the effects of transport stiffness are investigated, and results from additional simulations that were performed using a version of the SAT3 model which has been retuned to nonlinear gyrokinetic simulations closer to the transport threshold are shown. A discussion follows, including directions for future work.

# 2 Simulation setup

## 2.1 Experiment description

### 2.1.1 Ohmic cases

The Ohmic shots chosen for simulation in this work are 12 JET-ILW discharges in H, D and T. They are a subset of discharges that make up a 2.3 MA, 2.7 T LOC-SOC scan discussed in [40], where LOC ('Linear

[2]For high-power pulses, the reader is referred to [41] for a study validating the core transport predictions of TGLF-SAT2 for JET-ILW type-I ELMy H-modes across H, D and T.

Ohmic Confinement') refers to a regime in which the confinement time scales roughly linearly with density, $\tau_E \sim n_e$, and SOC ('Saturated Ohmic Confinement') describes a regime in which an increase in density has little to no effect on the confinement, $\tau_E \sim n_e^0$ [42]. A plot of confinement time against line-averaged density for these discharges is shown in figure 1. Note that these experiments demonstrate an anti-gyroBohm scaling of confinement with $\tau_{E,H} < \tau_{E,D} < \tau_{E,T}$ for cases of similar density.

For the purpose of our study, four groups of three discharges were selected from the scan, each containing three shots of comparable density in H, D and T, represented by the linked rings. The groups are labelled $1-4$ in order of increasing density, with group 1 in the LOC region, groups 3 and 4 in the SOC region, and group 2 around the transition point. Additional information for the pulses such as the shot number, the start time of the 0.5 s averaging window used for the HRTS measurements, the line-averaged density and the Ohmic power as measured by EFIT [43] is given in table 1, in which the labels a and b for the shot numbers correspond to different times in a given discharge.

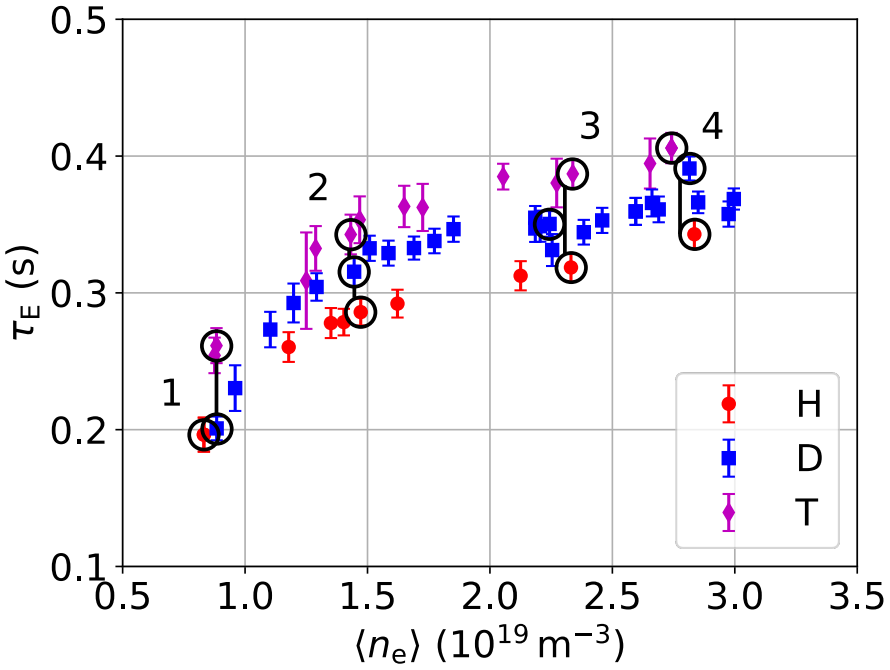


Figure 1: Energy confinement time against line-averaged electron density for a range of JET-ILW Ohmic discharges in H, D and T spanning a LOC-SOC transition. The four groups of similar-density shots in different isotopes considered in this work are marked by the connected rings, in order of increasing density.

### 2.1.2 L-mode cases

Three L-mode discharges were chosen, one in each hydrogenic isotope, with shot numbers #91450 (H), #89723 (D) and #99173 (T). These experiments were operated with a current of 2.5 MA and a magnetic field strength of 3.0 T, and were designed to have a similar line-averaged density and total stored energy, as demonstrated in figure 2. For the simulations of this work these experiments were analysed over a time window of $55-56$ s, as denoted by the dashed black boxes. NBI was used as an auxiliary heating mechanism with disparate values of the power required to achieve matched stored energy and density, with H at 4.38 MW, D at 3.20 MW and T at 1.45 MW, where the beam ions are the same as those of the bulk plasma. Through previous analysis, the H and D experiments were found to have a positive isotope scaling of the confinement time, $\tau_E \propto A^{0.15}$ [28] with the T discharge being performed later[3].

[3]Pulses #91450 (H) and #89723 (D) were conducted as part of a D and H campaign in 2016, with #99173 (T) being performed as part of DTE2 in 2021, and is not as well matched in terms of density and stored energy.

| Group | Pulse # | Time window start (s) | $\langle n_e \rangle$ $(10^{19}\mathrm{m}^{-3})$ | EFIT Ohmic Power (MW) |
|---|---|---|---|---|
| 1 | 91633 (H) | 53.41 | 0.83 | $1.30 \pm 0.01$ |
| | 96281 (D) | 59.01 | 0.88 | $1.28 \pm 0.06$ |
| | 100145 (T) | 53.11 | 0.88 | $1.12 \pm 0.02$ |
| 2 | 91637 (H) | 58.25 | 1.47 | $1.35 \pm 0.03$ |
| | 90633 (D) | 53.21 | 1.45 | $1.27 \pm 0.03$ |
| | 99263 (T) | 56.11 | 1.43 | $1.19 \pm 0.03$ |
| 3 | 91634a (H) | 55.91 | 2.33 | $1.60 \pm 0.02$ |
| | 97553 (D) | 56.21 | 2.24 | $1.54 \pm 0.03$ |
| | 100112a (T) | 56.11 | 2.34 | $1.44 \pm 0.03$ |
| 4 | 91634b (H) | 60.41 | 2.83 | $1.73 \pm 0.03$ |
| | 95766 (D) | 59.21 | 2.81 | $1.64 \pm 0.04$ |
| | 100112b (T) | 59.11 | 2.74 | $1.54 \pm 0.03$ |

Table 1: Experimental details of the 12 Ohmic cases considered in this work.

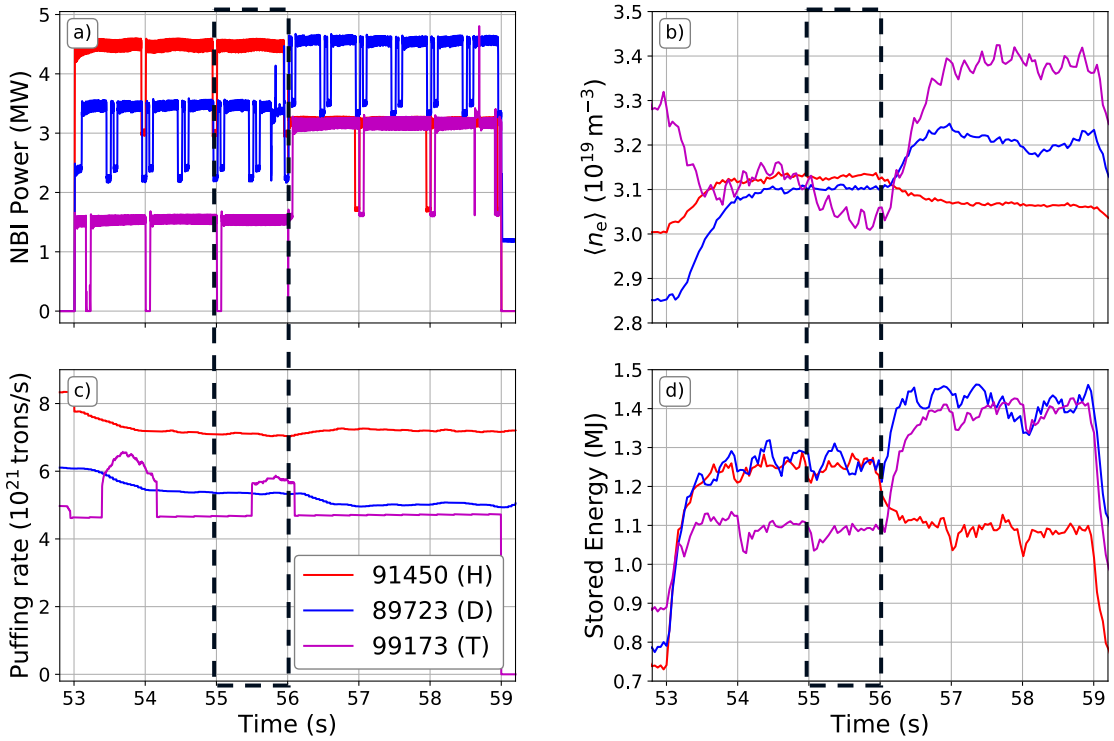


Figure 2: Experimental time-traces of the L-mode discharges, consisting of the NBI powers (a), line-averaged densities (b), gas puffing rates (c) and stored energies (d). The dashed black boxes represent the time window over which the shots were considered for our simulations.

## 2.2 Code settings

The integrated modelling was performed with JETTO-TGLF, where two types of simulation were considered. The first is 'interpretive', for which all quantities such as densities and temperatures retain their input profiles. The exception to this is the current profile which was evolved predictively, due to this not being routinely measured accurately. Interpretive simulations are a proxy for experiment, and form the basis of our comparisons. These results are labelled 'Interp.' in the plots to follow. The other type is 'predictive', in which the densities, temperatures and current are evolved via the transport equations of JETTO. For both types, rotation is treated interpretively. In all cases the simulations were run for a sufficient time such that the profiles reached a steady state. Across the minor radius 101 gridpoints were used, with an internal boundary condition being imposed at

$\rho_{\mathrm{tor}} = 0.85$, where $\rho_{\mathrm{tor}}$ is the square root of the normalised toroidal flux, for both the evolution of the profiles and the domain of the transport model. This allowed focus on the core transport, with less concern for the influence of the larger gradients in density that can appear near the tokamak edge.

The radial profiles used as an initial condition in JETTO for the Ohmic cases were imported via TRANSP [44]. The electron temperature and density profiles were measured using HRTS, for which a profile fitting example is shown in figure 3, and the ion temperature and rotation measurements were taken from main ion charge exchange using beam blips [45]. Owing to the purity of these discharges, shown in the analysis of [40], a value of $Z_{\mathrm{eff}} = 1.05$ was assumed in all Ohmic cases with a radially uniform interpretive Beryllium impurity, with residual hydrogenic impurities being sufficiently small to neglect in our simulations. Radiation was also neglected due to the relatively small values of radiative power measured via bolometry, $\mathcal{O}\,(0.1\,\mathrm{MW})$. In this work we are primarily interested in the isotope scaling of the confinement time $\tau_{\mathrm{E}}$, and particularly the influence of the transport model in its prediction. For Ohmic discharges, this is simply

$$\tau_{\mathrm{E}} = \frac{W}{P_{\mathrm{OH}}} \tag{1}$$

where $W$ is the stored energy of the plasma and $P_{\mathrm{OH}}$ is the Ohmic power. Given this interest, as well as the sensitivities associated with the calculation of $P_{\mathrm{OH}}$ and the nonlinear feedback mechanism this has on predictions when evolving the current profile, the total Ohmic power in the simulations of the Ohmic discharges was adjusted to match the total $P = VI$ value obtained from EFIT shown in the righthand column of table 1.

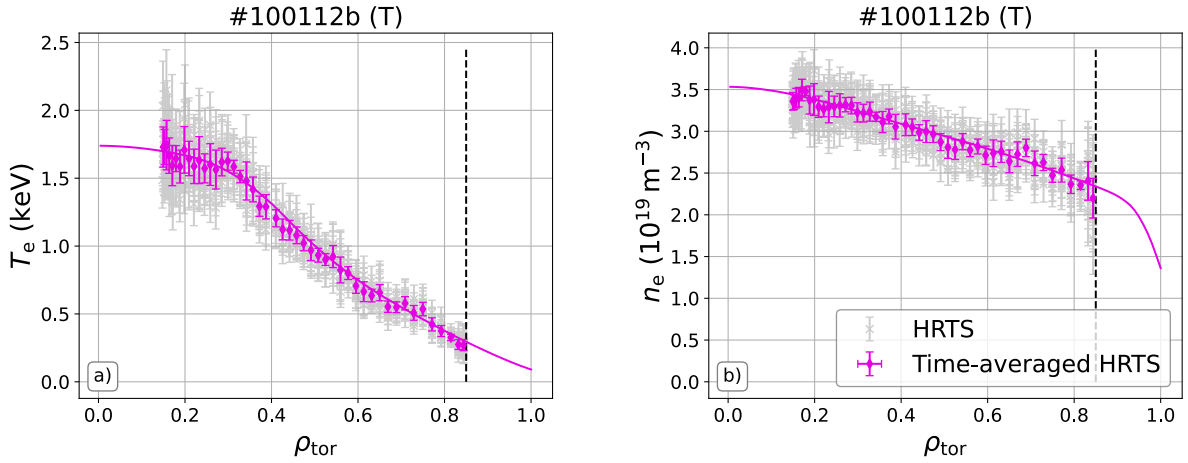


Figure 3: Example of HRTS data averaging and profile fitting for the electron temperature (a) and electron density (b) of pulse 100112b (see table 1). The raw data over the averaging window is shown in grey, the magenta data points are their time-averages at a given radial position, and the solid magenta line is the profile fit. The black dashed line indicates the boundary condition used in the simulations ($\rho_{\mathrm{tor}} = 0.85$), and the data for $\rho_{\mathrm{tor}} > 0.85$ is not shown.

For the L-modes, the electron density and temperature profiles were measured using HRTS and the rotation was determined from the best available diagnostic in operation during the pulse based on charge exchange spectroscopy measurements. The ion temperature profile of #99173 (T) was measured using main ion charge exchange, however this diagnostic was not available for the H and D discharges, and so for these $T_{\mathrm{i}} = T_{\mathrm{e}}$ was assumed within experimental uncertainties. For #99173, simulations with both the measured $T_{\mathrm{i}}$ and the assumption $T_{\mathrm{i}} = T_{\mathrm{e}}$ were performed. Due to the mass dependence of the electron-ion energy exchange term $P_{\mathrm{ei}} \propto (T_{\mathrm{e}} - T_{\mathrm{i}})/m_{\mathrm{i}}$ one would expect $T_{\mathrm{i}}$ to be closer to $T_{\mathrm{e}}$ for isotopes of lower mass, supporting this assumption. As will be seen however, the predictions made for #99173 using the two prescriptions of $T_{\mathrm{i}}$ exhibit minimal difference. An interpretive Beryllium impurity was again used for these discharges, with $Z_{\mathrm{eff}} = 1.1$ and $P_{\mathrm{rad}} = 0.5\,\mathrm{MW}$, motivated from bolometry measurements.

A continuous sawtooth model was applied for an additional source of transport within the $q = 1$ surface, with a standard diffusion coefficient of $0.3\,\mathrm{m^2 s^{-1}}$. The equilibrium was determined by EFIT at the start of the respective time windows and was not evolved throughout the simulations. The contribution of neoclassical

transport was calculated by NCLASS [46], however this was seen to be small in comparison to that of turbulent transport with $\chi_{\mathrm{i,neo}}/\chi_{\mathrm{i,turb}} \sim 0.03$ and $\chi_{\mathrm{e,neo}}/\chi_{\mathrm{e,turb}} \sim 10^{-2}$.

The NBI present in the L-modes was simulated using the PENCIL code [47] with the parameters used shown in table 2, noting again that the neutral beam species is the same as the main ion species of the discharge. Here, the octant refers to the position of one of the two neutral injector boxes around the torus, each of which houses eight positive ion neutral injectors (PINIs). Octant 4 was not used in shot #99173 over the time window considered.

| | NBI parameters (Octant 4, Octant 8) | | | |
|---|---|---|---|---|
| Pulse | Ion energy $E$ (keV) | Beam fraction with $(E, E/2, E/3)$ | PINIs used | Octant power (MW) |
| 91450 (H) | 61, 69 | $(0.31, 0.29, 0.39)$, $(0.31, 0.33, 0.36)$ | $(1,2,3,4,8)$, $(7,8)$ | 3.00, 1.38 |
| 89723 (D) | 83, 91 | $(0.5, 0.25, 0.25)$, $(0.51, 0.27, 0.22)$ | $(1,6)$ , $(7)$ | 2.09, 1.11 |
| 99173 (T) | -, 96.5 | -, $(0.55, 0.24, 0.21)$ | -, $(6,7)$ | -, 1.45 |

Table 2: Parameters for the NBI heating used in PENCIL for the L-mode simulations.

For the settings of TGLF within JETTO, the collision models chosen were those tuned to the corresponding saturation rules, namely XNU_MODEL = 2 was used with SAT1 and XNU_MODEL = 3 was used with SAT2 and SAT3. KYGRID_MODEL = 4 was selected for the wavenumber grid, with 12 binormal wavenumbers in the electron scale. KYGRID_MODEL = 4 uses 12 wavenumbers in the ion scale, with 10 evenly spaced between $k_y\rho_{\mathrm{i}} = 0.1$ and 1.0 and two additional wavenumbers at $k_y\rho_{\mathrm{i}} = 0.05, 0.15$ where $k_y$ is the binormal wavenumber and $\rho_{\mathrm{i}}$ is the ion gyroradius. The additional wavenumbers help better resolve the linear growth rate spectra at low $k_y$, which is important for accurately measuring quantities which play a crucial role in determining the saturated potential spectrum and hence calculating the turbulent transport. TGLF was run electrostatically, with electromagnetic field contributions proving negligible, and all other parameters were left at their default values. Within the $\rho_{\mathrm{tor}} = 0.85$ boundary, TGLF was called at 25 radial positions.

# 3 Integrated modelling simulation results

## 3.1 Profile predictions

The simulations described in the preceding section were performed each using SAT1-3. Considering first the low density Ohmic cases, predictions for the profiles of electron temperature, ion temperature and electron density for the shots of group 1 are shown in figure 4[4]. Here we see that the three saturation rules produce a similar electron temperature profile across isotope, exhibiting a common overprediction in this channel. The ion temperature predictions improve in the three models as one increases in isotope mass, with all overpredicting in H and all in approximate agreement for T. For the density, good agreement is found for the three saturation rules in H, which then becomes slightly underpredicted with increasing isotope mass.

The similarity of the electron temperature predictions may be somewhat contrary to expectation given the inclusion of the TEM branch of transport in SAT3, which in conditions of being TEM-dominated produces a differing saturation level to that obtained from ITG turbulence, which SAT1 and SAT2 use by default. To verify the existence of TEM modes in these simulations, figure 5a shows the dominant mode frequency at $k_y\rho_{\mathrm{i}} = 0.3$ obtained from the TGLF eigensolver as a function of $\rho_{\mathrm{tor}}$ for the three discharges of group 1, where a positive frequency denotes the electron diamagnetic direction and a negative frequency corresponds to the ion direction. The positive frequencies seen for the three discharges confirm that TEM is the dominant mode type around mid-radius[5], however we note the appearance of ITG modes as one approaches the boundary. These results suggest that the electron thermal transport for all models is not sufficiently stiff regardless of the saturation type. The question of transport stiffness will be returned to in Section 4.

[4]Note that only the experimental data inside the simulation boundary of $\rho_{\mathrm{tor}} = 0.85$ is shown.

[5]This mode labelling approximately matches the method used in SAT3, which considers the ratio of the linear energy flux between electrons and ions.

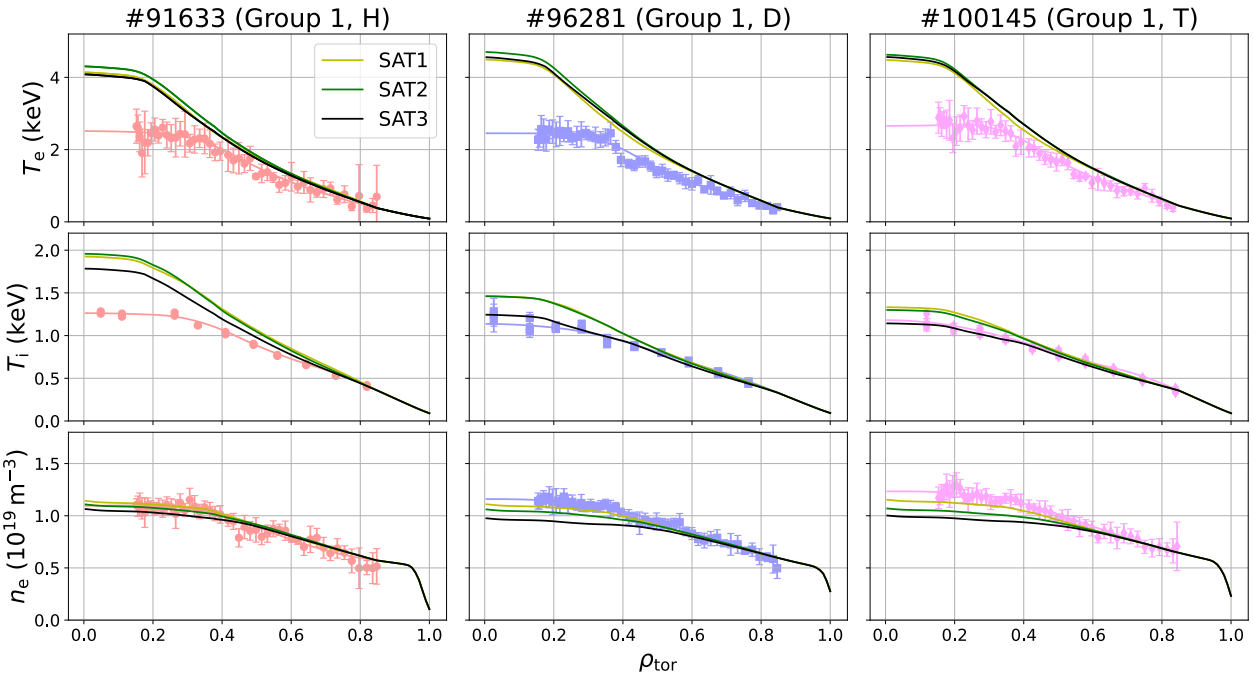


Figure 4: Profile predictions of JETTO-TGLF for SAT1 (yellow), SAT2 (green) and SAT3 (black) compared to experiment for the Ohmic shots of group 1. The electron temperature (row 1), ion temperature (row 2) and electron density (row 3) predictions are shown for the shots corresponding to H, D and T in columns 1-3 respectively.

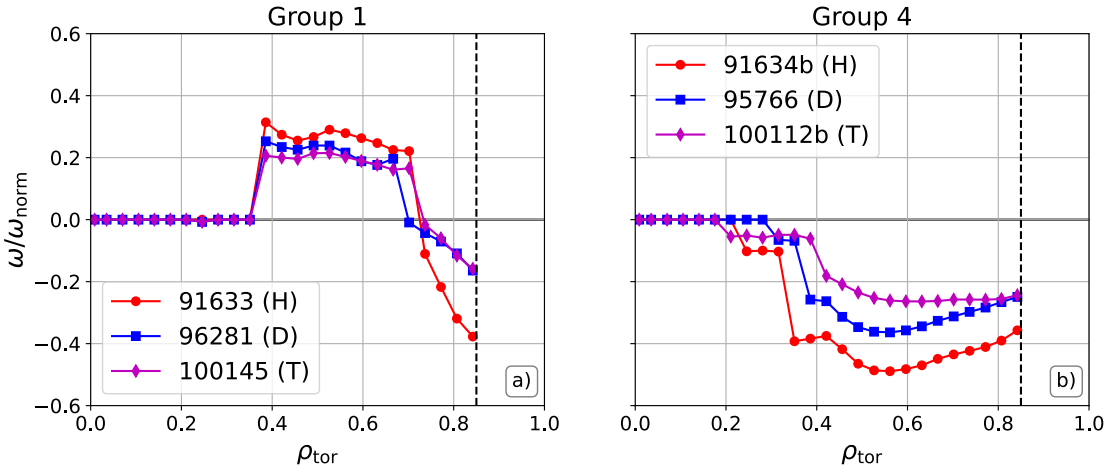


Figure 5: Dominant mode frequency at $k_y\rho_i = 0.3$ obtained from the TGLF eigensolver for flux surfaces present in the experimental profiles, for the different isotope discharges in Ohmic group 1 (a) and group 4 (b). Positive values of frequency indicate the electron diamagnetic direction while negative corresponds to the ion direction.

Turning to the higher density Ohmic cases, the analogous mode frequencies across $\rho_{tor}$ for Ohmic group 4 in figure 5b exhibit ITG modes across the radial domain. Profile predictions for this group are shown in figure 6, for which, similar to group 1, the electron temperature profiles are again seen to be overpredicted across isotopes and saturation models. In contrast however, the ion temperature predictions are now strongly overpredicted for all isotopes with almost identical predictions between models, and the density is seen to have approximate agreement for D and T however now with an overprediction in H. Previous integrated modelling studies of SOC discharges using TGLF have also found an overprediction of the ion temperature [48]. The similarity of the profile predictions of the different models is somewhat expected due to all using an ITG-based saturation level. The profile predictions for the remaining Ohmic cases, groups 2 and 3, are given in appendix A, demonstrating

progressive changes to the profiles as one transitions from group 1 to group 4.

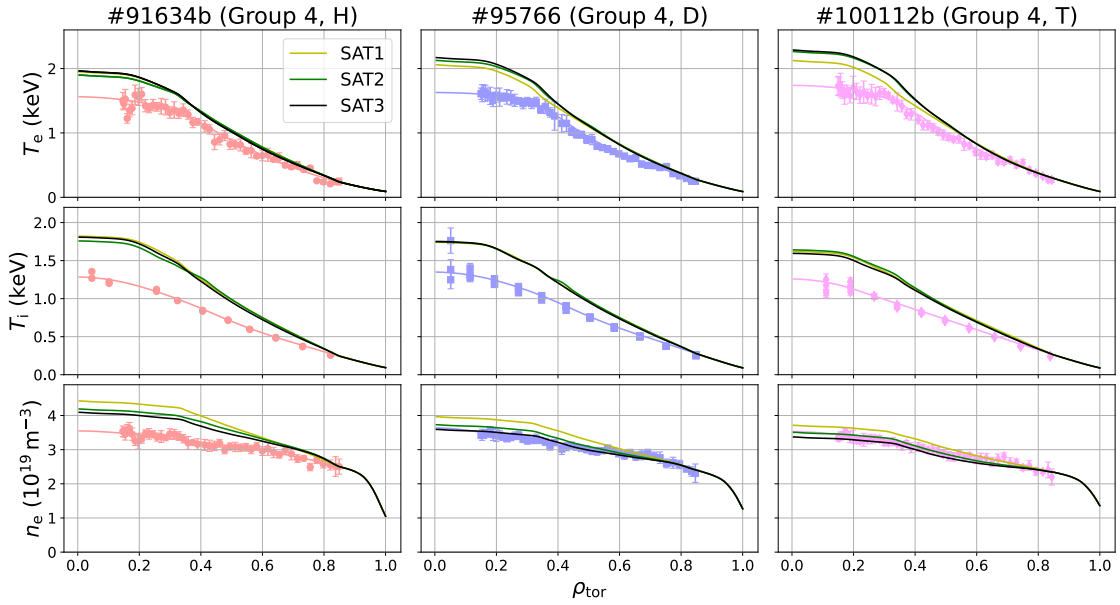


Figure 6: Profile predictions of JETTO-TGLF for Ohmic group 4, following the same layout as figure 4.

The profiles for the L-mode cases are shown in figure 7, where the simulations of #99173 have used $T_i = T_e$. Similar quality predictions are seen for the electron temperature and density channels as the Ohmic group 4 profiles, as may be expected for ITG-dominated cases of comparable densities, however here the ion temperature profile predictions are improved. This is likely due to the auxiliary heating leading to steeper gradients than the SOC cases, moving them away from the threshold and towards the area of parameter space TGLF was tuned to. This is discussed further in Section 4.1. The simulations of #99173 using the measured ion temperature profile are shown in figure 20, from which it can be seen that the predictions exhibit minimal sensitivity to this difference in initial condition.

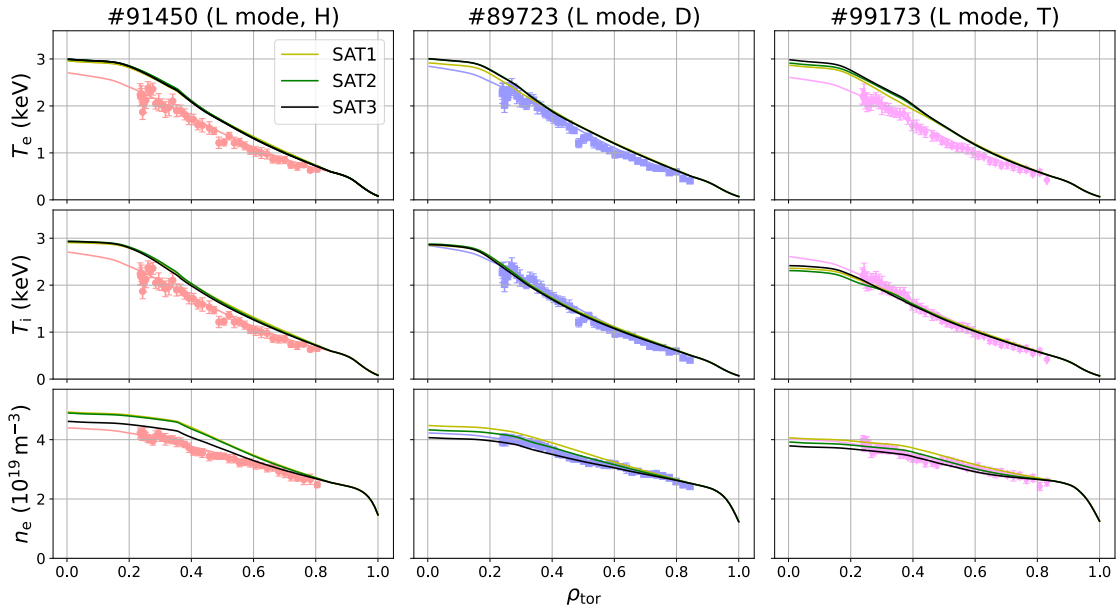


Figure 7: Profile predictions of JETTO-TGLF for the L-mode cases.

### 3.2 Confinement time predictions

Figure 8 plots the predicted confinement times of the different saturation models against the isotope mass of the discharges in each group, as well as the values of the confinement times obtained interpretively with which to compare. We note that these values are calculated over the whole plasma, and so are a measurement of the quality of the core confinement prediction given agreement in the edge region. For each group, the isotope scaling of confinement is similar across SAT1-3, as implied from the similarity of the profile predictions. A common trend across groups is that the scaling between D and T is typically well captured, as well as that between H and D for the low density Ohmic discharges of groups 1 and 2. As density increases however, to Ohmic groups 3 and 4 as well as the L-modes, the confinement of H becomes increasingly overpredicted relative to D and T. Moreover, there is a general overprediction in the magnitude of the confinement time across cases, on the order of 20%.

In the majority of cases the results of SAT3 are seen to be those closest to the interpretive, indicating greater levels of transport in comparison to the other saturation rules. Part of the reason for these observations is that the database of nonlinear gyrokinetic simulations SAT3 was trained on consisted of simulations of a higher resolution than were used for previous saturation rules, due to an observed increase in flux with increasing $k_y$ mode density until a point of convergence, such that SAT3 can predict a larger flux for equivalent conditions. This is described in appendix E.3 of [35]. Finally we note that, in line with the observations of figure 20, the predicted confinement time for #99173 in the L-modes is minimally changed by the inclusion of $T_\mathrm{i} \neq T_\mathrm{e}$.

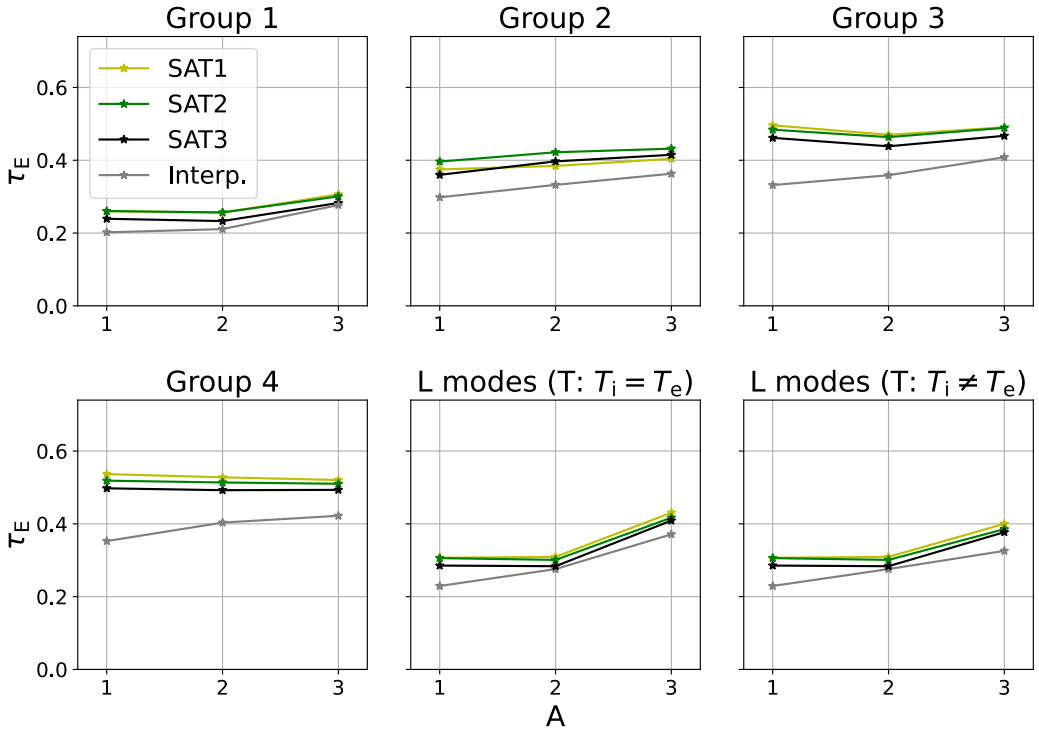


Figure 8: Predicted confinement times of SAT1 (yellow), SAT2 (green) and SAT3 (black) compared to interpretive values (grey) plotted against the isotope mass of the discharges in a given group. For example, group 1 (top left panel) plots the confinement times of shot #91633 at $A = 1$, #96281 at $A = 2$ and #100145 at $A = 3$ (see table 1). Groups 2-4 and the L-modes follow, for subplots reading left to right.

### 3.3 On the influence of ETG

The overprediction of confinement across models observed in the previous section, as well as the discrepancy for H in the cases of higher density, suggests that there are physical processes affecting the transport levels in our simulations that are not being accurately accounted for in our transport models. In previous work [49], a trio of discharges from the SOC branch of figure 1 was analysed using CGYRO-PORTALS [7], which uses ion-scale nonlinear CGYRO [50] for the transport model. This in principle produces the 'ground truth' that TGLF is attempting to replicate, albeit without the effects of electron-scale physics. The results of the preceding section echo the findings of the CGYRO-PORTALS study, in which good agreement was found for the three channels of the tritium discharge, however this was seen to worsen with decreasing isotope mass, originating primarily from the ion temperature channel. This is approximately borne out by figure 8, in the widening of the gap between the predictive and interpretive confinement times for groups 3 and 4 as one decreases from $A = 3$ to $A = 1$. As remarked in the study, observing this trend with ion-scale nonlinear gyrokinetics naturally makes transport mechanisms associated with electron-scale physics of interest, including ETG turbulence. Studies have shown that ETG turbulence can generate an anti-gyroBohm scaling effect of local transport [51], with the influence of electron-scale physics playing a larger role in lower mass isotope plasmas due to a decrease in scale separation.

To gauge the influence of electron-scale effects currently being described in our integrated modelling simulations, the Ohmic cases were simulated again with the TGLF contribution of ETG transport turned off, with the results of this exercise shown in figure 9. It is seen that the removal of ETG produces a negligible difference for the discharges of the lower density groups 1 and 2, and a small difference for the higher density groups of 3 and 4. It is emphasised that this is the TGLF prediction of electron-scale physics, and so may or may not agree with calculations from multiscale nonlinear gyrokinetic simulations. We note for example that the ETG model developed for use in TGLF was trained only on gyrokinetic simulations in pure D plasmas [19], and so isotope-dependent effects that occur in electron scale turbulence may be missing from our current ETG transport modelling prescription. Investigations into multiscale nonlinear gyrokinetic simulations in this regime should be carried out and compared with the predictions of TGLF, however this is beyond the scope of this paper and left to future work.

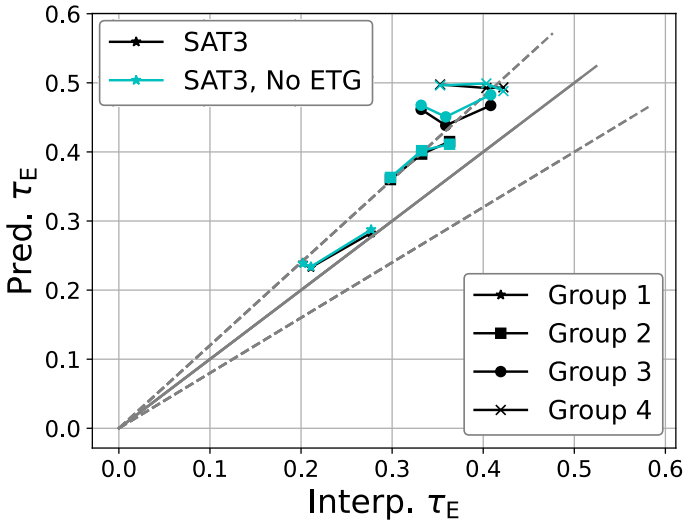


Figure 9: Prediction of the energy confinement time against interpretive values for JETTO-SAT3 of the 12 Ohmic cases (black) and those with the transport due to ETG turbulence turned off (cyan). They grey dashed lines indicate ±20% from the line $y = x$.

The suggestion of greater influence of multiscale effects for the higher density cases is supported by figure 10, which shows spectra obtained from linear CGYRO of the growth rate divided by $k_y$ for the $r/a = 0.5$ surface across the different isotope discharges for groups 1 and 4[6]. The spectrum of $\gamma_{k_y}/k_y$ typically exhibits two

[6]The input files for these simulations were automatically converted from the TGLF files obtained from JETTO using the

peaks, one in the ion scale and one in the electron scale, for which the relative heights of the peaks can be interpreted as a proxy for the importance of multiscale transport [53, 54]. Across isotopes it can be seen that the electron-scale peak height relative to the ion-scale increases as one changes from group 1 to 4, suggesting a possible increased relevance of ETG transport as one moves to these higher density cases.

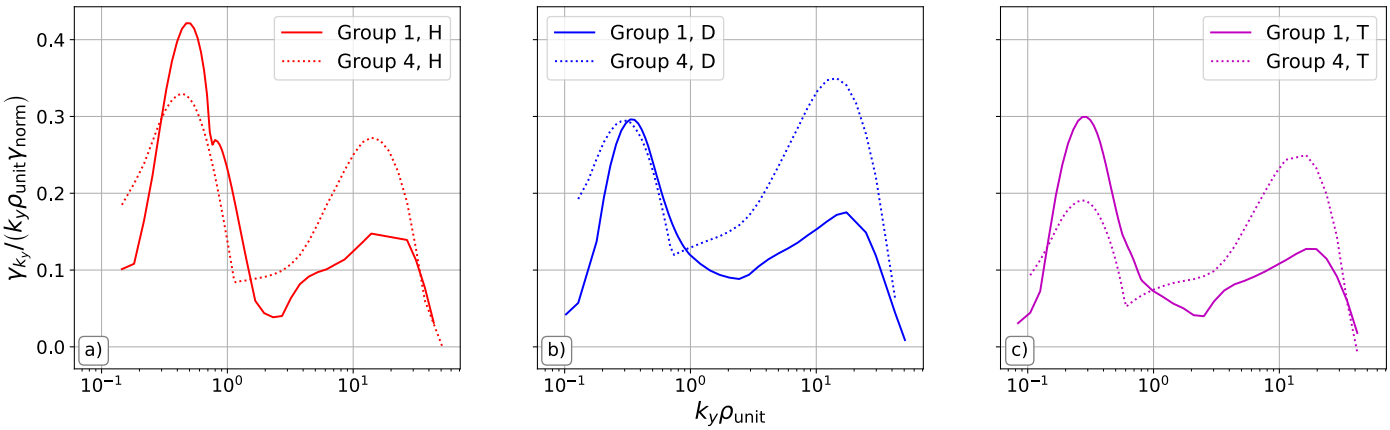


Figure 10: Linear CGYRO spectra of $\gamma_{k_y}/k_y$ against $k_y$ for a mid-radius surface $r/a = 0.5$ for Ohmic group 1 discharges (solid) and group 4 (dashed) of the corresponding H (a), D (b) and T (c) shots.

# 4 The effect of transport stiffness

## 4.1 Model considerations for temperature gradients close to threshold

During the course of this work, standalone TGLF simulations at different radial points across the experimental profiles were conducted to investigate the local properties of the turbulent transport, such as those of figure 5. For many of these simulations, heat fluxes were produced on the order of $\mathcal{O}(0-10)\ Q_{\text{GBD}}$, where $Q_{\text{GBD}}$ denotes gyroBohm heat flux units. Such fluxes are small relative to the database of simulations on which the saturation models of TGLF were tuned, with the GA-standard case [55], which forms the lynchpin of the tuning databases of SAT2 and SAT3, containing gradients far from threshold at $a/L_T = 3.0$ and having fluxes of around $Q_{\text{i}} \sim 50\, Q_{\text{GBD}}$. Owing to the stiff nature of tokamak transport [56] in which a critical gradient will typically be reached, in low power density experiments such as those simulated here one may expect to the transport model to be called primarily close to threshold, resulting in the smaller fluxes observed.

A consequence of this is that the tuning of the saturation model parameters may preferentially favour this above-threshold state, rather than those close to the critical gradient. This is illustrated in figure 11, showing a comparison between the heat fluxes obtained from nonlinear CGYRO simulations and a quasilinear model made up of linear CGYRO and the SAT3 model[7] across a scan of temperature gradient $a/L_T$[8]. This data was used as part of the tuning database of SAT3, with the input parameters other than temperature gradient corresponding to those of the GA-standard case.

The model shows strong agreement with the nonlinear gyrokinetic results for temperature gradients close to $a/L_T = 3.0$. However, closer to threshold, shown by the data points at $a/L_T = 1.5$ and $a/L_T = 2.25$, the model underpredicts the heat fluxes in both the ion and electron channel in comparison to those of nonlinear CGYRO. This observation of the underprediction of flux relative to higher fidelity models may offer an explanation as to the consistent overprediction in the confinement across the cases of Section 3, particularly in the temperature channels. That is, we may be finding that a steeper steady-state temperature profile is needed to satisfy power balance in our integrated modelling simulations as a result of our transport models being insufficiently stiff.

pyrokinetics software [52], and were run with the same resolutions as described in [21].

[7] By using linear gyrokinetic inputs instead of those used in reduced model eigensolvers, this ensures an accurate description of the linear physics consistent with the nonlinear simulations, giving greater clarity as to the properties of the saturation rule [57].

[8] The ion and electron temperature gradients were kept the same for the scan, $a/L_T = a/L_{T_{\text{i}}} = a/L_{T_{\text{e}}}$.

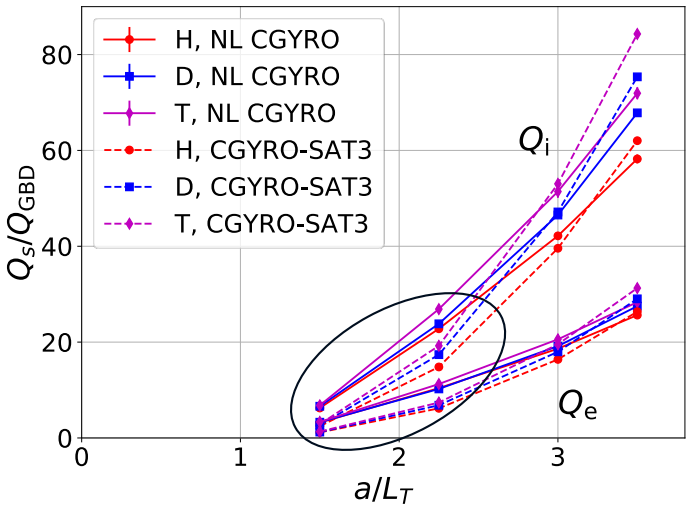


Figure 11: Turbulent heat fluxes for ions ($Q_\mathrm{i}$) and electrons ($Q_\mathrm{e}$) against temperature gradient ($a/L_T = a/L_{T_\mathrm{i}} = a/L_{T_\mathrm{e}}$) in H (red), D (blue) and T (magenta), with all other local input parameters being those of the GA-standard case. The solid lines are those obtained from nonlinear CGYRO simulations, while the dashed lines are the flux values obtained from combining the CGYRO linear solver with the SAT3 model. Figure adapted from [21].

### 4.2 Retuning the SAT3 model

To investigate the influence of this far-from-threshold tuning, we now consider retuning the parameters of SAT3 to only cases close to threshold. This ultimately amounts to replacing the original tuning database of SAT3 with the H, D and T $a/L_T = 1.5$ simulations with all other parameters being those of the GA-standard case, as well as a mid-radius nonlinear simulation of the L-mode H discharge #91450. This was included as it was a close-to-threshold case with parameters taken from the experimental profiles, exhibiting similar character to the $a/L_T = 1.5$ simulations. We note that this is an ad-hoc exercise and does not constitute an 'official' retuning of the SAT3 parameters.

To demonstrate what was changed, then focusing primarily on the ion-scale portion of the SAT3 model around where the spectrum peaks, the saturated potentials are modelled via [21]

$$\frac{\left\langle \left| \delta\hat{\phi}_{k_y} \right|^2 \right\rangle_{x,\theta,t}}{\Delta k_y} = \frac{\left\langle \left| \delta\hat{\phi}_{k_y=k_0} \right|^2 \right\rangle_{x,\theta,t}}{\Delta k_y} \left( \frac{\sigma_{k_y}}{\sigma_{k_y=k_0}} \right)^{c_1} \tag{2}$$

where

$$\frac{\sigma_{k_y}}{\sigma_{k_y=k_0}} = \left( -\frac{1}{2k_\mathrm{min}} k_y^2 + k_y + \frac{c}{b} \right) \Big/ \left( -\frac{1}{2k_\mathrm{min}} k_0^2 + k_0 + \frac{c}{b} \right) \qquad 0 < k_y \leq k_P \tag{3}$$

is a function describing the spectral shape, $k_P = 2k_\mathrm{min}$, $k_0 = 0.6k_\mathrm{min}$, $c_1$ is a constant and $\left\langle \left| \delta\hat{\phi}_{k_y=k_0} \right|^2 \right\rangle_{x,\theta,t} / \Delta k_y$ describes the saturation level. The description of the quantities $k_\mathrm{min}$, $c/b$, $c_1$ and $\left\langle \left| \delta\hat{\phi}_{k_y=k_0} \right|^2 \right\rangle_{x,\theta,t} / \Delta k_y$ using linear physics quantities $k_\mathrm{max}$ and $\gamma_\mathrm{max}$[9] in SAT3 are $k_\mathrm{min} = A_1 k_\mathrm{max}$ where $A_1 = 0.685$, $c/b = -0.751 k_\mathrm{max}$, $c_1 = -2.42$, and $\left\langle \left| \delta\hat{\phi}_{k_y=k_0} \right|^2 \right\rangle_{x,\theta,t} / \Delta k_y = A_2 \gamma_\mathrm{max}^2 B_\mathrm{unit}^2 / k_\mathrm{max}^5$ for ITG dominated cases, as the $a/L_T = 1.5$ simulations being considered here are, with $A_2 = 3.3$. The various numerical constants were obtained by fitting to the original database of nonlinear simulations. Here we fit them again, however only using the cases close to threshold.

[9] See figure 11 of [21].

An aspect of this exercise is shown in figure 12. In (a), the nonlinear CGYRO saturated potential spectra of different $a/L_T$ cases for an H plasma around the GA-standard case are shown. As the temperature gradient decreases, the peak of the potential spectrum moves to a higher $k_y\rho_{\text{unit}}$ value. In the SAT3 model, the position of this peak corresponds to the quantity $k_{\text{min}}$. In (b), the values of $k_{\text{min}}$ (triangles) and $c/b$ (stars) for the temperature gradient scans in H, D and T are shown, plotted against $k_{\text{max}}$. The joined lines are those of differing isotope but of the same temperature gradient, with the black markers indicating the #91450 simulation. The original value of $c/b$ in the SAT3 model can be seen to be a good fit for all cases across temperature gradient and isotope, and so is not retuned. However for $k_{\text{min}}$, the original fit of $0.685k_{\text{max}}$ can be seen to describe the higher temperature gradient cases (green and red) well, however the increasing of $k_{\text{min}}$ with lower temperature gradients seen in (a) means that the location of the peak of near-threshold cases is not as well captured (blue and orange). A re-fitting obtained from considering only the near-threshold cases is shown in dashed black, corresponding to $A_1 = 0.96$.

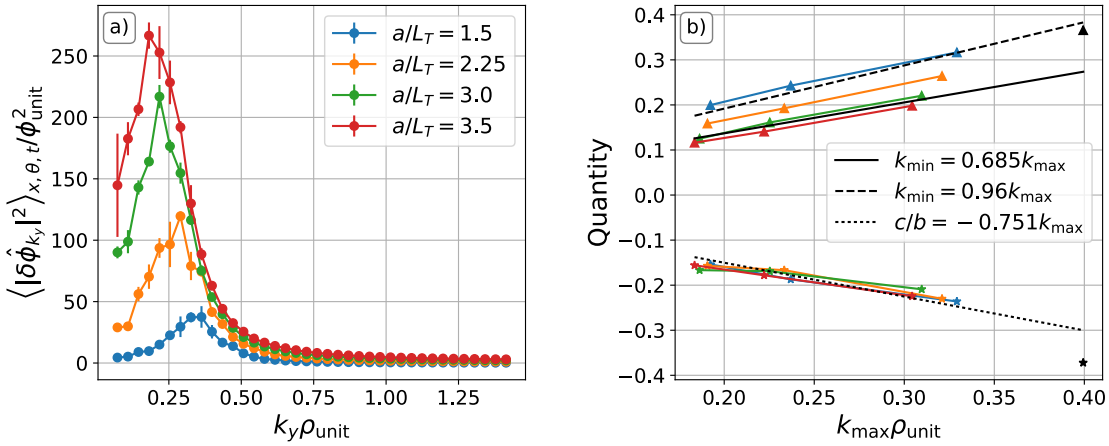


Figure 12: Saturated potential spectra (a) against binormal wave number for a range of different temperature gradient values around the GA-standard case for an H plasma. In (b), quantities that are used in SAT3 for modelling the spectral shape ($k_{\text{min}}$ and $c/b$) are shown against $k_{\text{max}}$ for the cases in (a), as well as the corresponding D and T spectra (not shown). Joined points of the same colour indicate those with the same temperature gradient but different isotopes. The black markers correspond to an additional simulation performed for a mid-radius surface of the L-mode shot #91450.

An analogous exercise was performed for the remaining fitted quantities, yielding $c_1 = -3.0$ and a change to the prefactor of the ITG dominated saturation level $A_2 = 4.0$. It is these three parameter changes that constitute the retuned SAT3 model, which for reference are summarised in table 3. Note that these changes will influence both the ITG and TEM branches.

| SAT3 parameter | Original value | Retuned value |
|---|---|---|
| $A_1$ | 0.685 | 0.96 |
| $A_2$ | 3.3 | 4.0 |
| $c_1$ | $-2.42$ | $-3.0$ |

Table 3: The parameter values changed in the process of retuning the SAT3 model to close-to-threshold cases. Note all other model parameters remained the same.

### 4.3 Retuned model results

With the retuned version of SAT3, the integrated modelling simulations of Section 3 were repeated. The previous plot of confinement time against isotope mass for the different saturation rules is now shown in figure 13 for the results of SAT3 and the retuned SAT3.

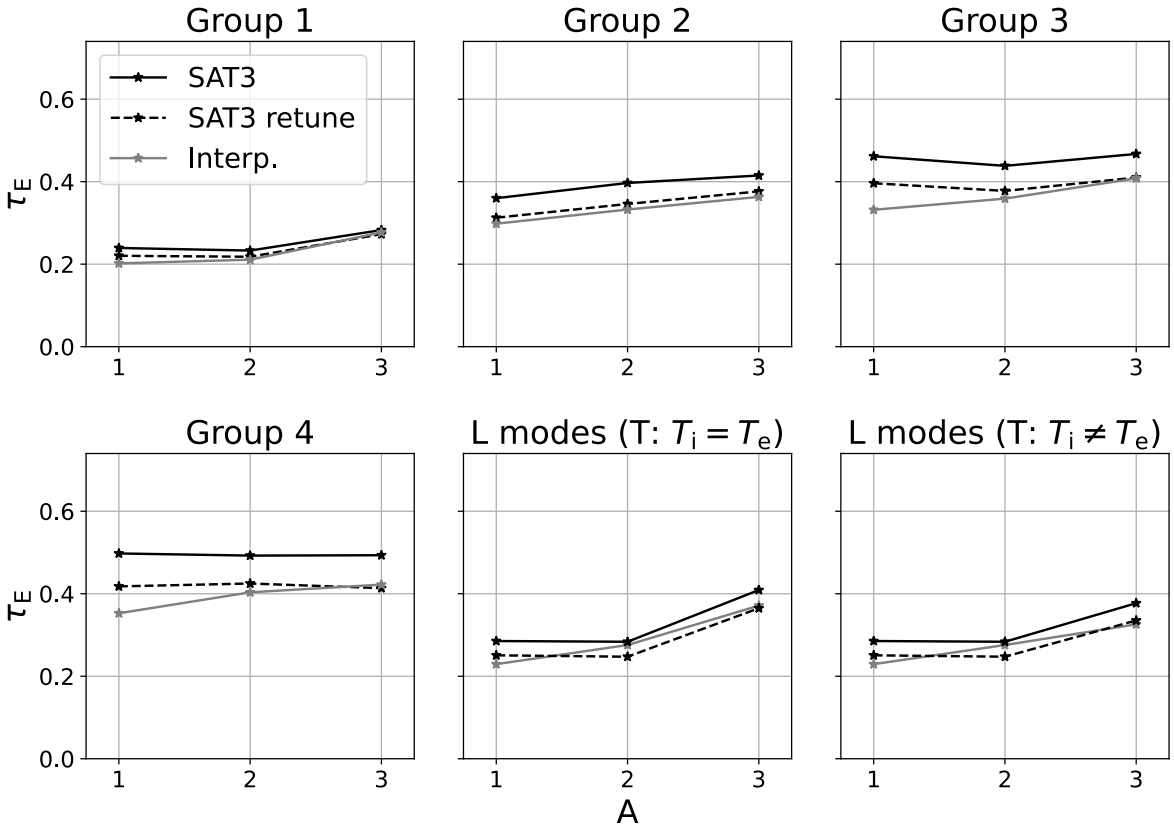


Figure 13: Predicted and interpretive confinement time against isotope mass of the respective discharges for the different groups, now with the results of the retuned version of SAT3 (dashed black).

A feature of note for the retuning is that the confinement time prediction has improved for all shots in all groups, decreasing its magnitude and bringing it much closer to that of the experimental values[10]. This arises from the retuned SAT3 model now predicting a greater level of transport close to the critical gradient relative to the original SAT3 model. While this change has improved the magnitude of the confinement prediction we note that the isotope scaling is unchanged, as evidenced by the black dashed data roughly being a vertical translation of the solid black data. This suggests that an increase in stiffness has not induced an additional isotope variation, such that the discrepancy between H and D in the higher density groups persists. In figure 14 this data is plotted against the line averaged densities of the simulations, further highlighting these features and demonstrating the recreation of the LOC-SOC transition.

How the confinement in each channel has been affected by this retuning can then be elucidated by considering the predicted profiles. For the Ohmic group 2 cases for example, the profile agreement can be seen to have improved across all channels and all isotopes, shown in figure 15. Here the previous overprediction of the temperature profiles has been brought to agreement for almost all discharges save for in the inner core, however this region is less important due to the relatively small volume it occupies, the ad-hoc nature of the sawtooth model, as well as the lack of transport that occurs with the shallow gradients present. We also note that despite a reduction in the temperature profiles, the density profile has changed minimally from its position of already-existing agreement.

[10]The exception to this is the L-mode D case, for which the original SAT3 was already in agreement with experiment (see middle column of figure 7), and now slightly underpredicts confinement.

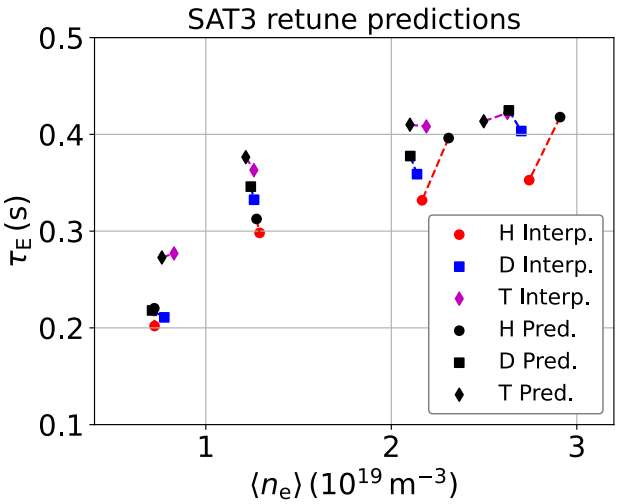


Figure 14: Predictions of confinement time against line averaged density for the SAT3 retune model compared with the interpretive results, where the predicted and interpretive values of a given case are joined by a dashed line.

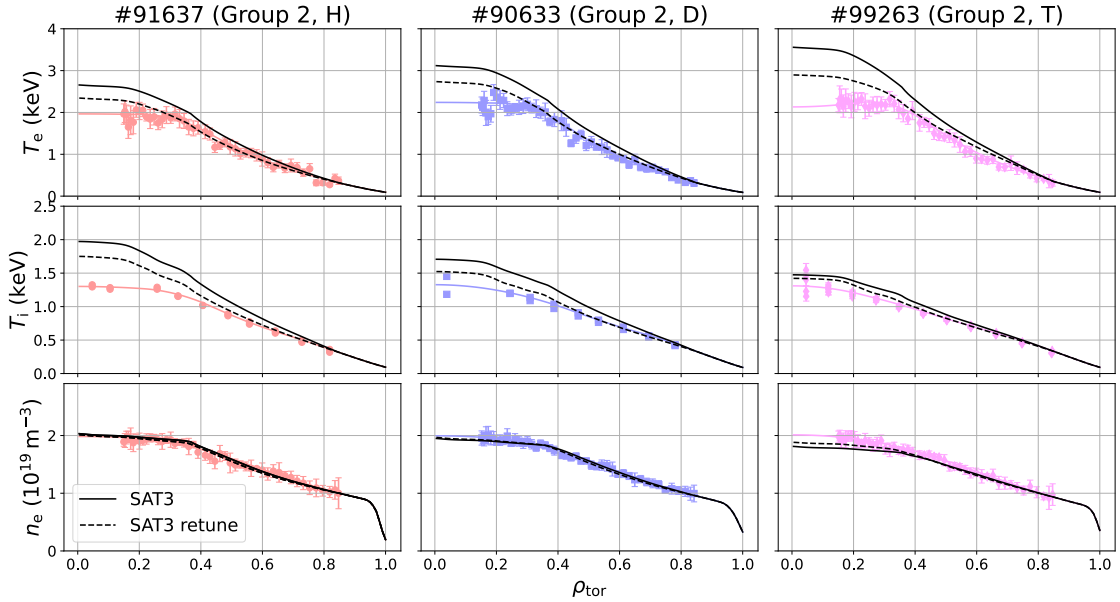


Figure 15: Profile predictions of JETTO-TGLF for the Ohmic group 2 cases including the retuned SAT3 model, following the same layout as figure 4.

In figure 16 the Ohmic group 4 cases demonstrate strong agreement for the electron temperature profiles. In D and T the density and ion temperature is also well modelled, however these channels continue to be overpredicted in H, causing the discrepancy in the confinement times previously observed. We note again that the H ion temperature was the channel most overpredicted for the CGYRO-PORTALS study. The updated profile predictions of Ohmic groups 1 and 3, which exhibit a combination of these considerations, are shown in appendix B. Finally, the L-mode predictions shown in figure 17 exhibit particularly good agreement across channels and discharges where again, the use of the measured $T_i$ profile causes minimal difference to the predictions (figure 23).

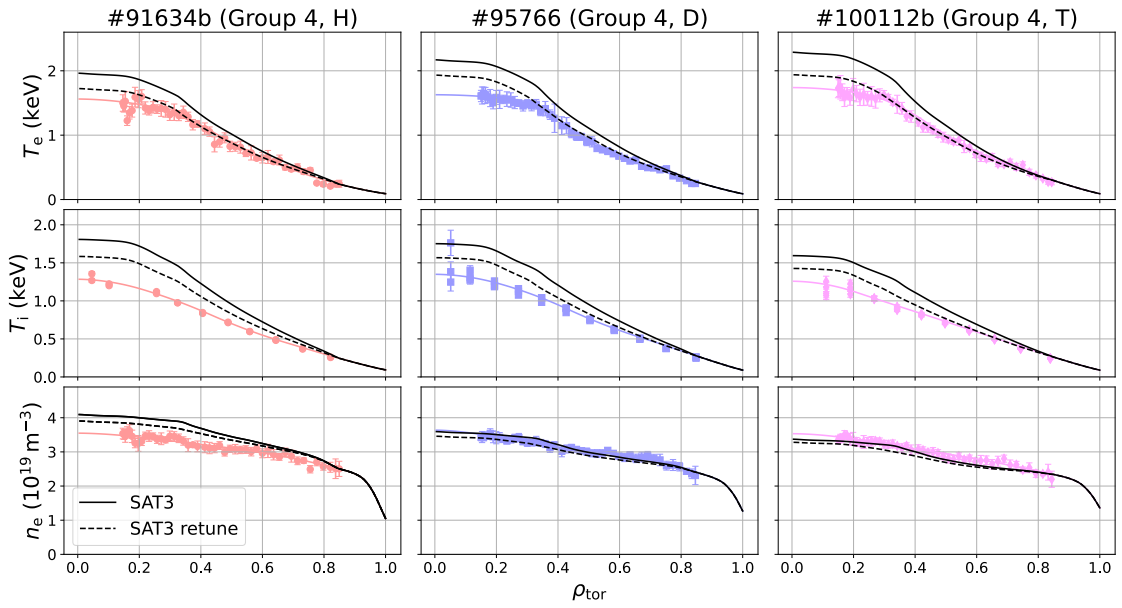


Figure 16: Profile predictions of JETTO-TGLF for the Ohmic group 4 cases including the retuned SAT3 model.

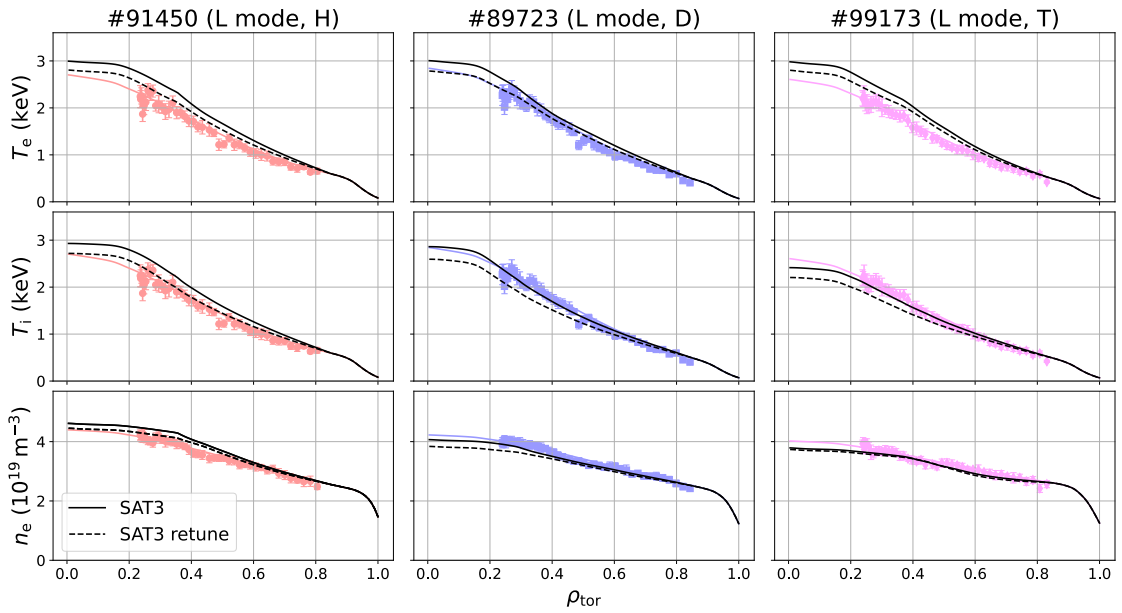


Figure 17: Profile predictions of JETTO-TGLF for the L-mode cases including the retuned SAT3 model.

## 5 Summary

In this work a validation study of JETTO-TGLF using the saturation rules SAT1-3 was performed on a selection of low power JET-ILW Ohmic and L-mode discharges in H, D and T, investigating their ability to recreate the isotope scaling of confinement observed in experiment. A consistent feature of the predictions was that the scaling was well-recreated between D and T across the discharges and across saturation rules. The scaling was also broadly well-captured between H and D for cases of low density, however as density increased so too did the discrepancy in the prediction for H, suggesting that transport processes relevant to these higher density cases that preferentially favour transport in lower isotope mass plasmas are currently missing from our transport models.

The overprediction in H has also been found in integrated modelling using ion-scale nonlinear gyrokinetics as the transport model, suggesting the influence of multiscale effects. While TGLF does include a description of

multiscale effects these have been tuned solely to deuterium plasmas, encouraging future comparisons between TGLF and multiscale nonlinear gyrokinetic simulations in different isotopes in the parameter regimes relevant to these SOC discharges. This should both shed light on the influence of ETG turbulence in the local transport properties of the discharges, as well as, if seen to be relevant, provide simulations for which the electron-scale parts of saturation rules can be updated to better include this physics.

A second consistent feature of the predictions was the overestimation of the confinement time across cases, on the order of 20%. This observation motivated an investigation into a retuning of the parameters of SAT3 solely to close-to-threshold cases, relevant to these low power discharges. The newly tuned model performed far better than its original counterpart, reducing the magnitude of the overprediction of the confinement time to almost agreement in the majority of cases. The H confinement still remained overpredicted in the higher density cases, supporting the need for the aforementioned multiscale comparisons. Due to its tuning database being far from threshold the original SAT3 model is hypothesised to perform better in cases of significant heating, which will be tested in future work. To avoid situations of input-power-dependent saturation rules, in future a greater focus on quasilinear transport models' performance close to threshold is encouraged in an attempt to find a sufficiently general description of the turbulent transport. This could be done via greater representation of such cases in future tuning databases, or preferentially, the implementation of a theory-based model to account for the behaviour of the model close to threshold, such as that described in [58].

# 6 Acknowledgements

This work has been carried out within the framework of the EUROfusion Consortium, funded by the European Union via the Euratom Research and Training Programme (Grant Agreement No 101052200 — EUROfusion). Views and opinions expressed are however those of the authors only and do not necessarily reflect those of the European Union or the European Commission. Neither the European Union nor the European Commission can be held responsible for them. This work has been part-funded by the EPSRC Energy Programme [grant number EP/W006839/1]. To obtain further information on the data and models underlying this paper please contact PublicationsManager@ukaea.uk. The authors also gratefully acknowledge access to the CINECA High-Performance Computer MARCONI.

# A Integrated modelling profile predictions

Here for reference the JETTO-TGLF predictions of Ohmic groups 2 and 3 using SAT1-3 are shown in figures 18 and 19 respectively, as well as the predictions of the L-mode T discharge #99173 with and without the assumption $T_i = T_e$ in figure 20.

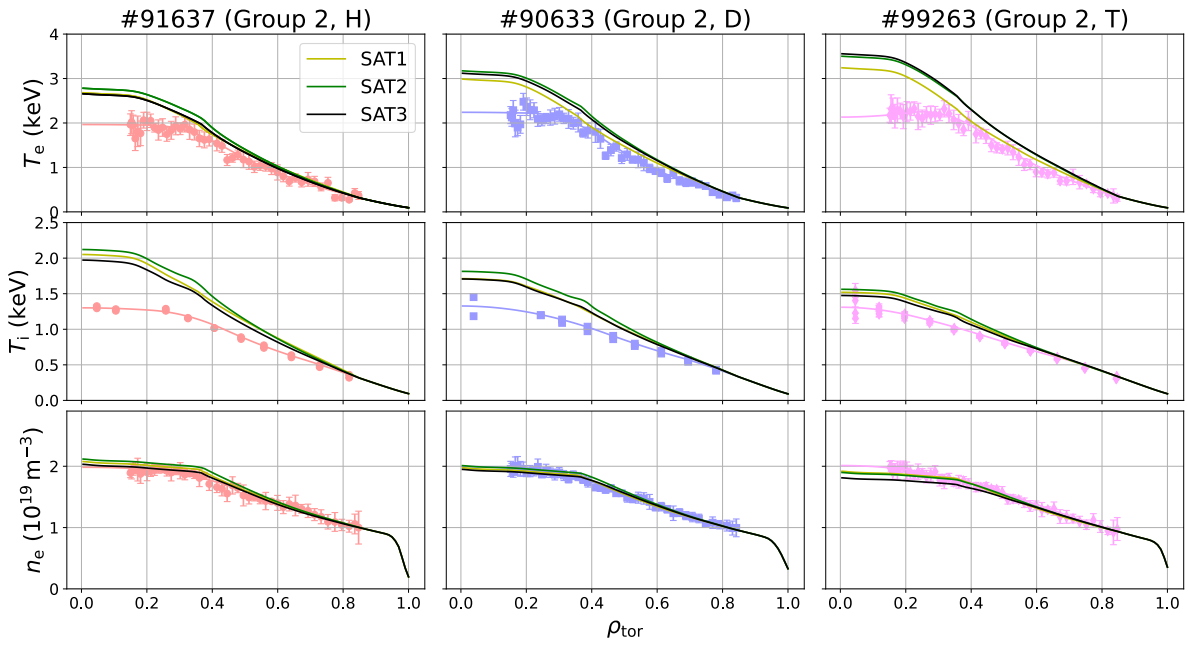


Figure 18: Profile predictions of JETTO-TGLF for the Ohmic group 2 cases, following the same layout as figure 4.

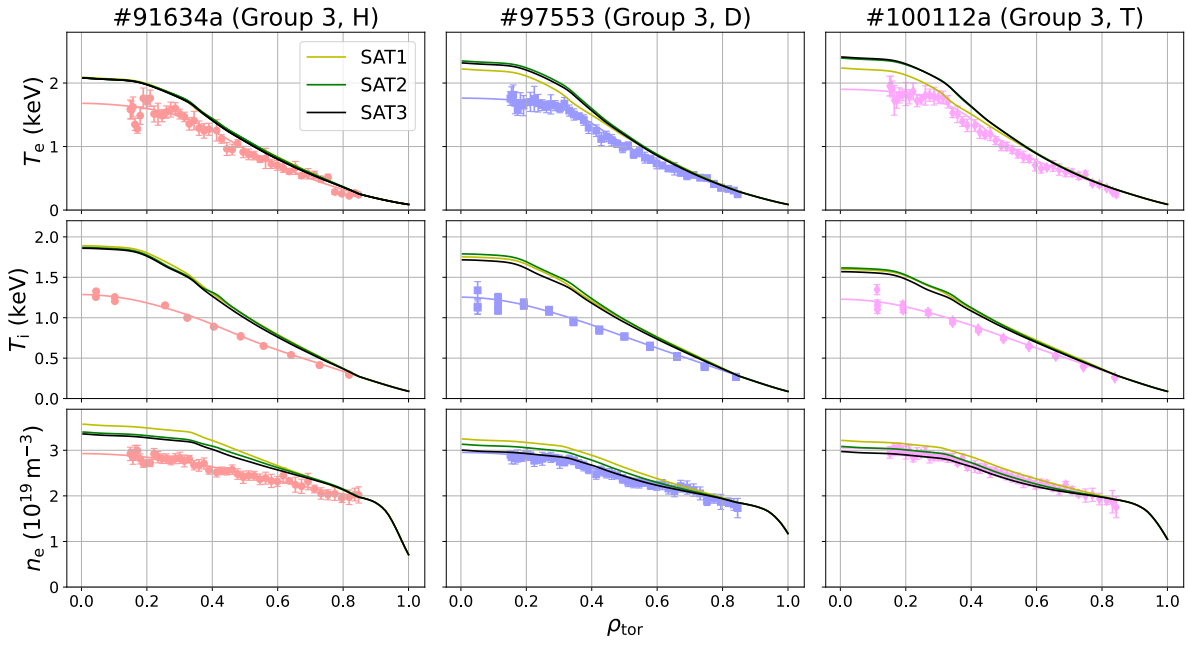


Figure 19: Profile predictions of JETTO-TGLF for the Ohmic group 3 cases.

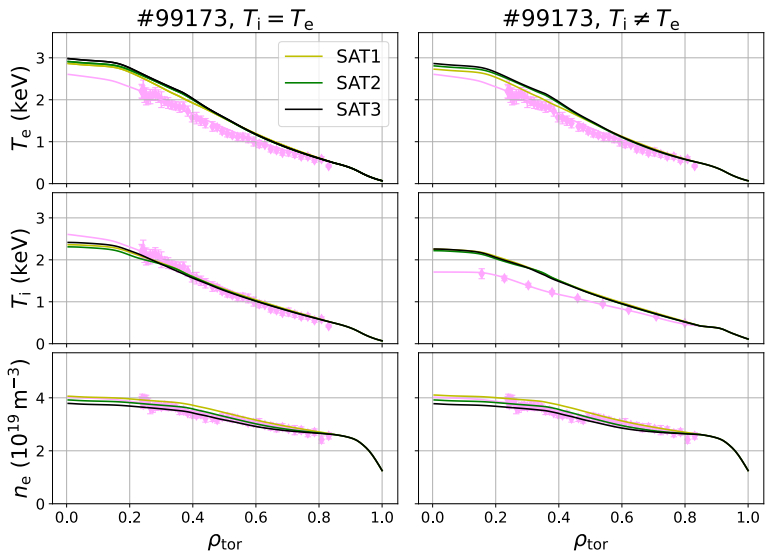


Figure 20: Profile predictions of JETTO-TGLF for L-mode shot #99173 with and without $T_i = T_e$.

# B Integrated modelling profile predictions with retuned SAT3

Here for reference we show the profile predictions of Ohmic groups 2 and 3 including the retuned SAT3 model, in figures 21 and 23 respectively, as well as the predictions of the L-mode T discharge #99173 with and without the assumption $T_i = T_e$ in figure 23.

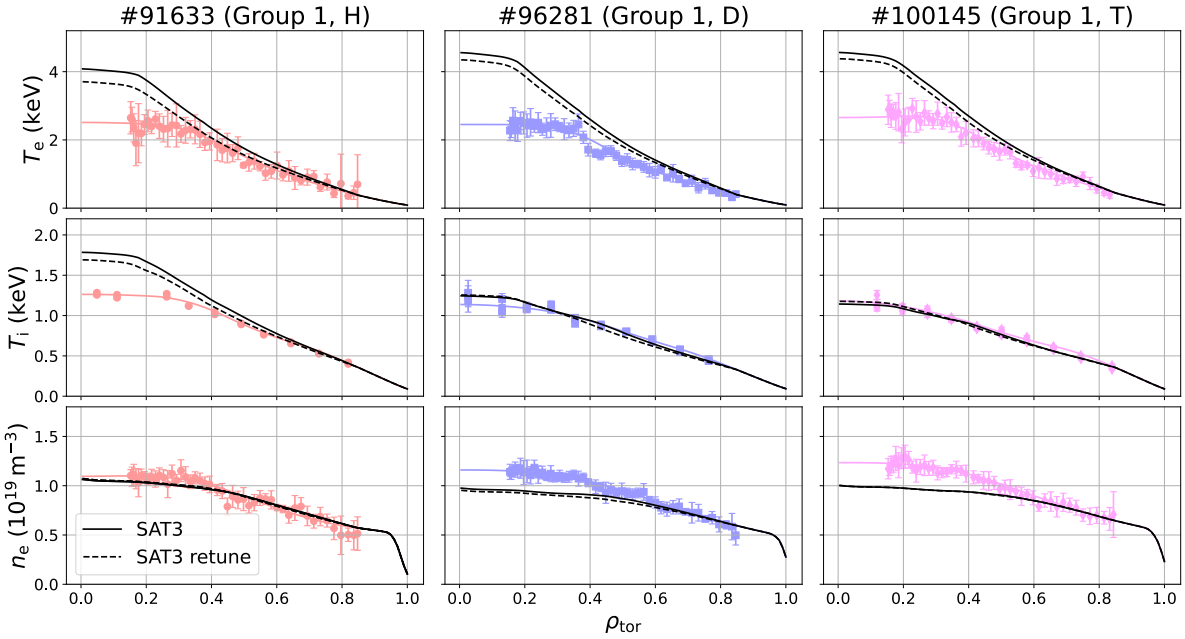


Figure 21: Profile predictions of JETTO-TGLF for the Ohmic group 1 cases now including the retuned SAT3 model, following the same layout as figure 4.

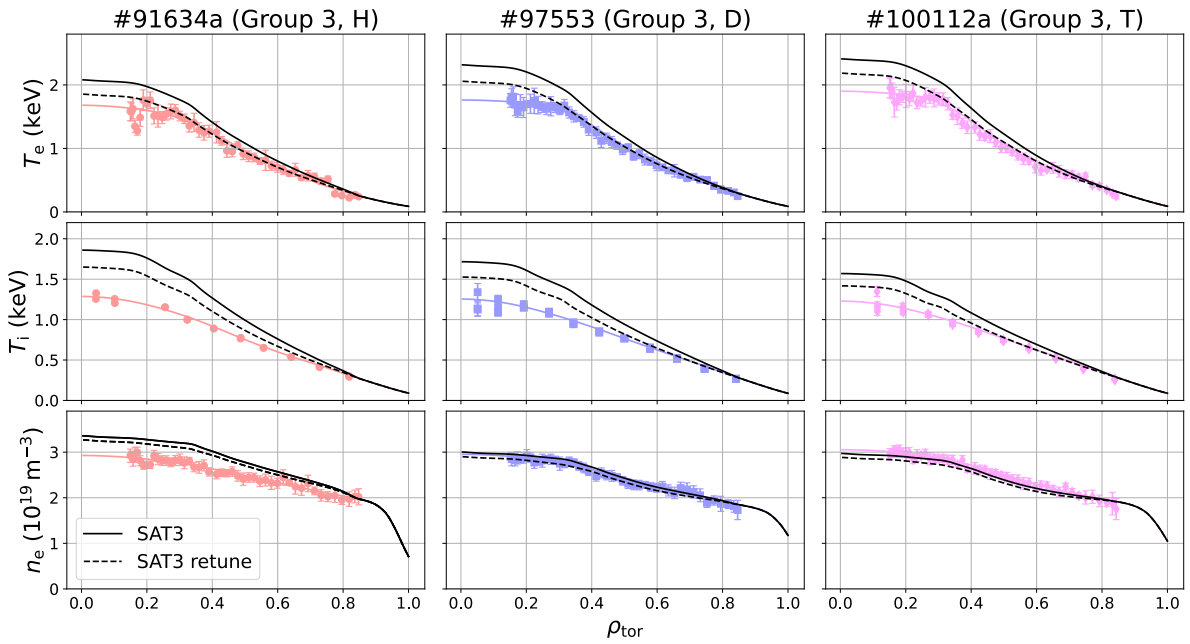


Figure 22: Profile predictions of JETTO-TGLF for the Ohmic group 3 cases, now including the retuned SAT3 model.

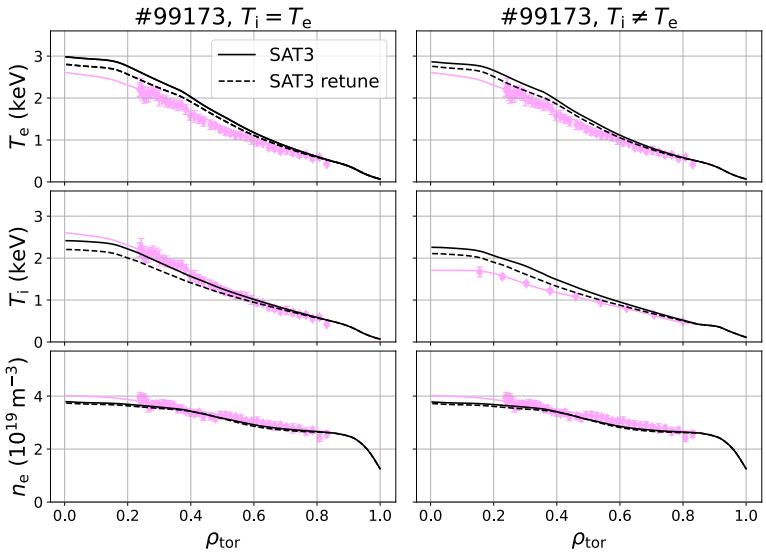


Figure 23: Profile predictions of JETTO-TGLF for #99173 with and without $T_i = T_e$, now including the retuned SAT3 model.

## References


[1]G. Cenacchi and A. Taroni, *Jetto: a free boundary plasma transport code*, 1988.

[2]G. V. Pereverzev and P. N. Yushmanov, *ASTRA - automated system for TRansport analysis*, 2002.

[3]C. Bourdelle, "Integrated modelling of tokamak plasmas: progress and challenges towards ITER operation and reactor design", Plasma Physics and Controlled Fusion **67**, Publisher: IOP Publishing, 043001 (2025).

[4]A. J. Brizard and T. S. Hahm, "Foundations of nonlinear gyrokinetic theory", Reviews of Modern Physics **79**, Publisher: American Physical Society, 421–468 (2007).

[5]X. Garbet, Y. Idomura, L. Villard, and T. H. Watanabe, "Gyrokinetic simulations of turbulent transport", Nuclear Fusion **50**, Publisher: IOP Publishing, 043002 (2010).

[6]A. Di Siena, A. Bañón Navarro, T. Luda, G. Merlo, M. Bergmann, L. Leppin, T. Görler, J. Parker, L. LoDestro, T. Dannert, K. Germaschewski, B. Allen, J. Hittinger, B. Dorland, G. Hammett, and F. Jenko, "Global gyrokinetic simulations of ASDEX upgrade up to the transport timescale with GENE–tango", Nuclear Fusion **62**, 106025 (2022).

[7]P. Rodriguez-Fernandez, N. Howard, A. Saltzman, S. Kantamneni, J. Candy, C. Holland, M. Balandat, S. Ament, and A. White, "Enhancing predictive capabilities in fusion burning plasmas through surrogate-based optimization in core transport solvers", Nuclear Fusion **64**, Publisher: IOP Publishing, 076034 (2024).

[8]M. Erba, T. Aniel, V. Basiuk, A. Becoulet, and X. Litaudon, "Validation of a new mixed bohm/gyro-bohm model for electron and ion heat transport against the ITER, tore supra and START database discharges", Nuclear Fusion **38**, 1013 (1998).

[9]C. Bourdelle, J. Citrin, B. Baiocchi, A. Casati, P. Cottier, X. Garbet, and F. I. and, "Core turbulent transport in tokamak plasmas: bridging theory and experiment with QuaLiKiz", Plasma Physics and Controlled Fusion **58**, Publisher: IOP Publishing, 014036 (2015).

[10]J. Citrin, C. Bourdelle, F. J. Casson, C. Angioni, N. Bonanomi, Y. Camenen, X. Garbet, L. Garzotti, T. Görler, O. Gürcan, F. Koechl, F. Imbeaux, O. Linder, K. v. d. Plassche, P. Strand, G. Szepesi, and JET Contributors, "Tractable flux-driven temperature, density, and rotation profile evolution with the quasilinear gyrokinetic transport model QuaLiKiz", Plasma Physics and Controlled Fusion **59**, 124005 (2017).

[11]G. M. Staebler, J. E. Kinsey, and R. E. Waltz, "Gyro-landau fluid equations for trapped and passing particles", Physics of Plasmas **12**, Publisher: American Institute of Physics, 102508 (2005).

[12]G. M. Staebler, J. E. Kinsey, and R. E. Waltz, "A theory-based transport model with comprehensive physics", Physics of Plasmas **14**, Publisher: American Institute of Physics, 055909 (2007).

[13]G. M. Staebler and J. E. Kinsey, "Electron collisions in the trapped gyro-landau fluid transport model", Physics of Plasmas **17**, 122309 (2010).

[14]A. Casati, C. Bourdelle, X. Garbet, F. Imbeaux, J. Candy, F. Clairet, G. Dif-Pradalier, G. Falchetto, T. Gerbaud, V. Grandgirard, Ö. D. Gürcan, P. Hennequin, J. Kinsey, M. Ottaviani, R. Sabot, Y. Sarazin, L. Vermare, and R. E. Waltz, "Validating a quasi-linear transport model versus nonlinear simulations", Nuclear Fusion **49**, Publisher: IOP Publishing, 085012 (2009).

[15]K. L. van de Plassche, J. Citrin, C. Bourdelle, Y. Camenen, F. J. Casson, V. I. Dagnelie, F. Felici, A. Ho, S. Van Mulders, and JET Contributors, "Fast modeling of turbulent transport in fusion plasmas using neural networks", Physics of Plasmas **27**, 022310 (2020).

[16]A. Ho, J. Citrin, C. Bourdelle, Y. Camenen, F. J. Casson, K. L. van de Plassche, H. Weisen, and JET Contributors, "Neural network surrogate of QuaLiKiz using JET experimental data to populate training space", Physics of Plasmas **28**, 032305 (2021).

[17]L. Zanisi, A. Ho, J. Barr, T. Madula, J. Citrin, S. Pamela, J. Buchanan, F. Casson, V. Gopakumar, and J. E. T. Contributors, "Efficient training sets for surrogate models of tokamak turbulence with active deep ensembles", Nuclear Fusion **64**, Publisher: IOP Publishing, 036022 (2024).

[18]C. Stephens, X. Garbet, J. Citrin, C. Bourdelle, K. van de Plassche, and F. Jenko, "Quasilinear gyrokinetic theory: a derivation of QuaLiKiz", Journal of Plasma Physics **87**, 905870409 (2021).

[19]G. M. Staebler, J. Candy, N. T. Howard, and C. Holland, "The role of zonal flows in the saturation of multi-scale gyrokinetic turbulence", Physics of Plasmas **23**, Publisher: American Institute of Physics, 062518 (2016).

[20]G. M. Staebler, E. A. Belli, J. Candy, J. E. Kinsey, H. Dudding, and B. Patel, "Verification of a quasi-linear model for gyrokinetic turbulent transport", Nuclear Fusion **61**, Publisher: IOP Publishing, 116007 (2021).

[21]H. G. Dudding, F. J. Casson, D. Dickinson, B. S. Patel, C. M. Roach, E. A. Belli, and G. M. Staebler, "A new quasilinear saturation rule for tokamak turbulence with application to the isotope scaling of transport", Nuclear Fusion **62**, Publisher: IOP Publishing, 096005 (2022).

[22]S. M. Kaye, J. W. Connor, and C. M. Roach, "Thermal confinement and transport in spherical tokamaks: a review", Plasma Physics and Controlled Fusion **63**, Publisher: IOP Publishing, 123001 (2021).

[23]M. Giacomin, D. Kennedy, F. J. Casson, A. C J, D. Dickinson, B. S. Patel, and C. M. Roach, "On electromagnetic turbulence and transport in STEP", Plasma Physics and Controlled Fusion **66**, Publisher: IOP Publishing, 055010 (2024).

[24]*STEP - spherical tokamak for energy production*, (June 19, 2024) `https://step.ukaea.uk/` (visited on 04/13/2025).

[25]M. Giacomin, D. Dickinson, W. Dorland, N. Mandell, A. Bokshi, F. Casson, H. Dudding, D. Kennedy, B. Patel, and C. Roach, "A quasi-linear model of electromagnetic turbulent transport and its application to flux-driven transport predictions for STEP", Journal of Plasma Physics **91**, E16 (2025).

[26]S. D. Scott, M. C. Zarnstorff, C. W. Barnes, R. Bell, N. L. Bretz, C. Bush, Z. Chang, D. Ernst, R. J. Fonck, L. Johnson, E. Mazzucato, R. Nazikian, S. Paul, J. Schivell, E. J. Synakowski, H. Adler, M. Bell, R. Budny, E. Fredrickson, B. Grek, A. Janos, D. Johnson, D. McCune, H. Park, A. Ramsey, M. H. Redi, G. Taylor, M. Thompson, and R. Wieland, "Isotopic scaling of confinement in deuterium–tritium plasmas", Physics of Plasmas **2**, Publisher: American Institute of Physics, 2299–2307 (1995).

[27]"ITER physics basis expert groups on confinement and transport and confinement modelling and database, ITER physics basis editors, chapter 2: plasma confinement and transport", Nuclear Fusion **39**, Publisher: IOP Publishing, 2175–2249 (1999).

[28]C. F. Maggi, H. Weisen, J. C. Hillesheim, A. Chankin, E. Delabie, L. Horvath, F. Auriemma, I. S. Carvalho, G. Corrigan, J. Flanagan, L. Garzotti, D. Keeling, D. King, E. Lerche, R. Lorenzini, M. Maslov, S. Menmuir, S. Saarelma, A. C. C. Sips, E. R. Solano, E. Belonohy, F. J. Casson, C. Challis, C. Giroud, V. Parail, C. Silva, and M. V. and, "Isotope effects on l-h threshold and confinement in tokamak plasmas", Plasma Physics and Controlled Fusion **60**, Publisher: IOP Publishing, 014045 (2018).

[29]H. Weisen, C. F. Maggi, M. Oberparleiter, F. J. Casson, Y. Camenen, S. Menmuir, L. Horvath, F. Auriemma, T. W. Bache, N. Bonanomi, A. Chankin, E. Delabie, L. Frassinetti, J. Garcia, C. Giroud, D. King, R. Lorenzini, M. Marin, P. A. Schneider, P. Siren, J. Varje, and E. Viezzer, "Isotope dependence of energy, momentum and particle confinement in tokamaks", Journal of Plasma Physics **86**, 905860501–undefined (2020).

[30]T. Tala, A. Järvinen, C. Maggi, P. Mantica, A. Mariani, A. Salmi, I. Carvalho, A. Chomiczewska, E. Delabie, F. Devasagayam, J. Ferreira, W. Gromelski, N. Hawkes, L. Horvath, J. Karhunen, D. King, A. Kirjasuo, E. Kowalska-Strzeciwilk, S. Leerink, M. Lennholm, B. Lomanowski, M. Maslov, S. Menmuir, R. Morales, R. Sharma, H. Sun, K. Tanaka, and J. E. T. Contributors, "Isotope mass scaling and transport comparison between JET deuterium and tritium l-mode plasmas", Nuclear Fusion **63**, Publisher: IOP Publishing, 112012 (2023).

[31]G. Manfredi and M. Ottaviani, "Gyro-bohm scaling of ion thermal transport from global numerical simulations of ion-temperature-gradient-driven turbulence", Physical Review Letters **79**, Publisher: American Physical Society, 4190–4193 (1997).

[32]J. Garcia, T. Görler, F. Jenko, and G. Giruzzi, "Gyrokinetic nonlinear isotope effects in tokamak plasmas", Nuclear Fusion **57**, Publisher: IOP Publishing, 014007 (2017).

[33]J. Garcia, R. J. Dumont, J. Joly, J. Morales, L. Garzotti, T. W. Bache, Y. Baranov, F. J. Casson, C. Challis, K. Kirov, J. Mailloux, S. Saarelma, M. Nocente, A. Banon-Navarro, T. Goerler, J. Citrin, A. Ho, D. Gallart, and M. M. and, "First principles and integrated modelling achievements towards trustful fusion power predictions for JET and ITER", Nuclear Fusion **59**, Publisher: IOP Publishing, 086047 (2019).

[34]E. A. Belli, J. Candy, and R. E. Waltz, "Reversal of turbulent gyroBohm isotope scaling due to nonadiabatic electron drive", Physics of Plasmas **26**, Publisher: American Institute of Physics, 082305 (2019).

[35]H. G. Dudding, "A new quasilinear saturation rule for tokamak turbulence", PhD thesis (University of York, Oct. 2022).

[36]P. Rodriguez-Fernandez, N. T. Howard, A. Saltzman, L. Shoji, T. Body, D. J. Battaglia, J. W. Hughes, J. Candy, G. M. Staebler, and A. J. Creely, "Core performance predictions in projected SPARC first-campaign plasmas with nonlinear CGYRO", Physics of Plasmas **31**, 062501 (2024).

[37]J. McClenaghan, A. Marinoni, A. O. Nelson, T. Neiser, L. L. Lao, G. M. Staebler, S. P. Smith, O. M. Meneghini, B. C. Lyons, P. B. Snyder, and M. Austin, "Examining transport and integrated modeling predictive capabilities for negative-triangularity scenarios", Plasma Physics and Controlled Fusion **66**, Publisher: IOP Publishing, 115008 (2024).

[38]J. Hughes, P. Rodriguez-Fernandez, A. Hubbard, D. Battaglia, M. Miller, A. Cavallaro, N. Howard, T. Wilks, and A. Creely, "High confinement regimes on SPARC: operational conditions for access and avoidance", Nuclear Fusion **65**, Publisher: IOP Publishing, 052001 (2025).

[39]C. L. Rettig, T. L. Rhodes, J. N. Leboeuf, W. A. Peebles, E. J. Doyle, G. M. Staebler, K. H. Burrell, and R. A. Moyer, "Search for the ion temperature gradient mode in a tokamak plasma and comparison with theoretical predictions", Physics of Plasmas **8**, 2232–2237 (2001).

[40]M. Nave, E. Delabie, J. Ferreira, J. Garcia, D. King, M. Lennholm, B. Lomanowski, F. Parra, P. Fernandez, J. Bernardo, M. Baruzzo, M. Barnes, F. Casson, J. Hillesheim, A. Hubber, E. Joffrin, A. Kappatou, C. Maggi, A. Mauriya, L. Meneses, M. Romanelli, F. Salzedas, and J. E. T. Contributors, "Isotope effects on intrinsic rotation in hydrogen, deuterium and tritium plasmas", Nuclear Fusion **63**, Publisher: IOP Publishing, 044002 (2023).

[41]P. Schneider, C. Angioni, F. Auriemma, N. Bonanomi, T. Görler, R. Henriques, L. Horvath, D. King, R. Lorenzini, H. Nyström, M. Maslov, J. Ruiz, G. Szepesi, C. Challis, A. Chomiczewska, E. Delabie, J. Fontdecaba, L. Frassinetti, J. Garcia, C. Giroud, J. Hillesheim, J. Hobirk, A. Kappatou, D. Keeling, E. Kowalska-Strzeciwilk, M. Lennholm, B. Lomanowski, T. Luda di Cortemiglia, C. Maggi, S. Menmuir, G. Pucella, A. Thorman, and J. E. T. Contributors, "Isotope physics of heat and particle transport with tritium in JET-ILW type-i ELMy h-mode plasmas", Nuclear Fusion **63**, Publisher: IOP Publishing, 112010 (2023).

[42]J. E. Rice, J. Citrin, N. M. Cao, P. H. Diamond, M. Greenwald, and B. A. Grierson, "Understanding LOC/SOC phenomenology in tokamaks", Nuclear Fusion **60**, Publisher: IOP Publishing, 105001 (2020).

[43]L. L. Lao, H. S. John, R. D. Stambaugh, A. G. Kellman, and W. Pfeiffer, "Reconstruction of current profile parameters and plasma shapes in tokamaks", Nuclear Fusion **25**, Publisher: IOP Publishing, 1611 (1985).

[44]R. Hawryluk, "An empirical approach to tokamak transport", in Physics of plasmas close to thermonuclear conditions (1981).

[45]E. Delabie, M. M. F. Nave, P. Rodriguez-Fernandez, B. Lomanowski, M. Lennholm, and JET Contributors Team, "Energy confinement in ohmic discharges in h, d and t on JET-ILW", **2021**, Conference Name: APS Division of Plasma Physics Meeting Abstracts ADS Bibcode: 2021APS..DPPCO7003D, CO07.003 (2021).

[46]W. A. Houlberg, K. C. Shaing, S. P. Hirshman, and M. C. Zarnstorff, "Bootstrap current and neoclassical transport in tokamaks of arbitrary collisionality and aspect ratio", Physics of Plasmas **4**, Publisher: American Institute of Physics, 3230–3242 (1997).

[47]C. D. Challis, J. G. Cordey, H. Hamnén, P. M. Stubberfield, J. P. Christiansen, E. Lazzaro, D. G. Muir, D. Stork, and E. Thompson, "Non-inductively driven currents in JET", Nuclear Fusion **29**, Publisher: IOP Publishing, 563–570 (1989).

[48]I. Erofeev, E. Fable, C. Angioni, R. McDermott, and T. A. U. Team, "Theory-based modeling of LOC–SOC transitions in ASDEX upgrade", Nuclear Fusion **57**, Publisher: IOP Publishing, 126067 (2017).

[49]P. Rodriguez-Fernandez, H. Howard N.T., A. Saltzman, S. Kantamneni, A. White, E. Delabie, B. Lomanowski, T. Biewer, J. Candy, C. Holland, M. Nave, J. Garcia, M. Lennholm, and J. Contributors, "Core performance predictions with nonlinear gyrokinetics and implications to scope burning-plasma tokamaks", in (Sept. 2023).

[50]J. Candy, E. A. Belli, and R. V. Bravenec, "A high-accuracy eulerian gyrokinetic solver for collisional plasmas", Journal of Computational Physics **324**, 73–93 (2016).

[51]N. T. Howard, C. Holland, A. E. White, M. Greenwald, and J. Candy, "Fidelity of reduced and realistic electron mass ratio multi-scale gyrokinetic simulations of tokamak discharges", Plasma Physics and Controlled Fusion **57**, Publisher: IOP Publishing, 065009 (2015).

[52]B. S. Patel, P. Hill, L. Pattinson, M. Giacomin, A. Bokshi, D. Kennedy, H. G. Dudding, J. F. Parisi, T. F. Neiser, A. C. Jayalekshmi, D. Dickinson, and J. R. Ruiz, "Pyrokinetics - a python library to standardise gyrokinetic analysis", Journal of Open Source Software **9**, 5866 (2024).

[53]A. J. Creely, P. Rodriguez-Fernandez, G. D. Conway, S. J. Freethy, N. T. Howard, A. E. White, and t. A. U. Team, "Criteria for the importance of multi-scale interactions in turbulent transport simulations", Plasma Physics and Controlled Fusion **61**, Publisher: IOP Publishing, 085022 (2019).

[54]M. R. Hardman, M. Barnes, and C. M. Roach, "Stabilisation of short-wavelength instabilities by parallel-to-the-field shear in long-wavelength $E \times B$ flows", Journal of Plasma Physics **86**, 905860601 (2020).

[55]R. E. Waltz, G. M. Staebler, W. Dorland, G. W. Hammett, M. Kotschenreuther, and J. A. Konings, "A gyro-landau-fluid transport model", Physics of Plasmas **4**, Publisher: American Institute of Physics, 2482–2496 (1997).

[56]P. A. Schneider, A. Bustos, P. Hennequin, F. Ryter, M. Bernert, M. Cavedon, M. G. Dunne, R. Fischer, T. Görler, T. Happel, V. Igochine, B. Kurzan, A. Lebschy, R. M. McDermott, P. Morel, and M. Willensdorfer, "Explaining the isotope effect on heat transport in l-mode with the collisional electron-ion energy exchange", Nuclear Fusion **57**, Publisher: IOP Publishing, 066003 (2017).

[57]B. Patel, "Confinement physics for a steady state net electric burning spherical tokamak", PhD thesis (University of York, Jan. 2021).

[58]M. Pueschel, P.-Y. Li, and P. Terry, "Predicting the critical gradient of ITG turbulence in fusion plasmas", Nuclear Fusion **61**, Publisher: IOP Publishing, 054003 (2021).